



Trovarelli, Federico (2022) *Strategies for attitude control of reconfigurable modular spacecraft*. MSc(R) thesis.

<https://theses.gla.ac.uk/82678/>

Copyright and moral rights for this work are retained by the author

A copy can be downloaded for personal non-commercial research or study, without prior permission or charge

This work cannot be reproduced or quoted extensively from without first obtaining permission in writing from the author

The content must not be changed in any way or sold commercially in any format or medium without the formal permission of the author

When referring to this work, full bibliographic details including the author, title, awarding institution and date of the thesis must be given

Enlighten: Theses

<https://theses.gla.ac.uk/>  
[research-enlighten@glasgow.ac.uk](mailto:research-enlighten@glasgow.ac.uk)



University  
of Glasgow

# Strategies for Attitude Control of Reconfigurable Modular Spacecraft

Submitted January 2022, in partial fulfilment of the conditions for the award of the degree **Master of Science by Research**.

**Federico Trovarelli**

**Supervised by Prof Colin McInnes**

James Watt School of Engineering

University of Glasgow

I hereby declare that this dissertation is all my own work, except as indicated in the text:

Signature \_\_\_\_\_

Date 23 / 01 / 2022

I hereby declare that I have all necessary rights and consents to publicly distribute this dissertation via the University of Glasgow e-dissertation archive.

Public access to this dissertation is restricted until: \_\_\_ / \_\_\_ / \_\_\_\_\_



## Abstract

The purpose of this thesis is to propose, investigate and develop an innovative approach to the attitude control of Cubesat-sized, modular and variable-shape spacecraft. These systems could ideally comply with the requirements of a larger variety of in-orbit functions and better adapt to the needs of specific subsystems in achieving and maintaining the desired attitude.

The reference array is assumed to consist of a certain number of modules interconnected by means of revolute joints. One interesting aspect, which is the specific focus of the present thesis, is that such system can be capable of exploiting the dynamic effect of momentum conserving internal torques generated by the modules rotating with respect to each other for reorientation purposes. Initial inspiration for this proposed approach to spacecraft attitude control design has been drawn from the study of the well-known '*falling cat*' problem.

In the long term, this innovative attitude control methodology, could justify the increase in cost and complexity modular reconfigurable systems require not only with advantages in the added versatility with respect to the mission tasks but also with better performance in attitude control system efficiency, accuracy, stability and even robustness.

Specifically, this thesis discusses the available information present in literature about momentum preserving attitude control of multibody arrays and possible space applications, builds and validates a tool for the investigation of the peculiarities of these systems and finally investigates their non-linear behaviour for both the 2D and 3D cases. With respect to previous work in the field, optimal attitude control trajectories that take into account module impingement are discussed and the dynamics of momentum-preserving manoeuvres is analysed from the physical and mathematical points of view for both 2D and 3D manoeuvres. The results of the analysis demonstrate the validity of the concept and highlighted some the potentialities but also the critical points for a further development of the technology.



## Acknowledgements

I hereby take this opportunity to thank my thesis supervisor, Colin McInnes, for helping directing my efforts. He taught me a lot in any sense and was always patient and supportive.

Also, I would like to thank the friends I grew up with in all the phases of my youth. Each of them has influenced somehow the person that I am now.

A special thank goes to my parents Marco and Francesca, who were always present when I needed them, to my sister Chiara, that will be my best friend for all my life, and to my grandparents, Bianca Maria, Nazareno, Magda and Lorenzo, who indirectly remind me where I come from.



# Contents

<b>Abstract</b>	<b>i</b>
<b>Acknowledgements</b>	<b>iii</b>
<b>1 Introduction</b>	<b>1</b>
1.1 The Reconfigurable Spacecraft . . . . .	1
1.2 Internal Torques for Attitude Control . . . . .	3
1.3 Thesis Overview . . . . .	4
1.4 Published work . . . . .	5
<b>2 Mechanics Background</b>	<b>6</b>
2.1 Reference Frames & Transformations . . . . .	6
2.2 Planar Multibody Mechanics . . . . .	9
2.3 3D Multibody Mechanics . . . . .	12
<b>3 Simulator Development</b>	<b>19</b>
3.1 Planar Model Model Simulator . . . . .	19
3.1.1 Validation & Verification . . . . .	19
3.1.2 Implementation Aspects . . . . .	20
3.2 3D Model Simulator . . . . .	20
3.2.1 Validation & Verification . . . . .	21
3.2.2 Implementation Aspects . . . . .	24
3.3 Other Tools . . . . .	25
3.3.1 Closed-Loop Feedback Control . . . . .	25
3.3.2 Pseudospectral Local Optimization . . . . .	26
3.3.3 Newton-Raphson Root Estimation Method . . . . .	26
3.3.4 Collision Maps . . . . .	27
<b>4 Results</b>	<b>29</b>
4.1 Planar Reorientation Trajectories . . . . .	29

4.1.1	Optimal Control Trajectories . . . . .	30
4.1.2	Rectangular Trajectories . . . . .	32
4.2	3D Reorientation Trajectories . . . . .	36
<b>5</b>	<b>Conclusions &amp; Recommendations</b>	<b>40</b>
5.1	Conclusions . . . . .	40
5.2	Recommendations . . . . .	41
	<b>Bibliography</b>	<b>43</b>

# List of Figures

1.1	Multipanel cubic spacecraft. . . . .	3
2.1	Classical angles $\theta$ , $\phi$ , $\psi$ relating body $B$ - and inertial $I$ -frames [19] <small>[used with permission]</small> . . . . .	7
2.2	Reference frame transformation from $\mathbf{A}$ to $\mathbf{B}$ [19] <small>[used with permission]</small> . . . . .	8
2.3	Planar array of 3 interconnected rods ( $Z$ -axes pointing out-of-plane). . . . .	9
2.4	L-shape multipanel system with local reference frames. . . . .	13
3.1	Typical revolute joint motion. . . . .	21
3.2	2-panel pendulum in constant gravitational field, conditions at $t = 0$ [s]. . . . .	22
3.3	3-panel pendulum in constant gravitational field, conditions at $t = 0$ [s]. . . . .	22
3.4	Total energy variation for a 2-panel pendulum oscillating in constant gravity field. . . . .	22
3.5	Total energy variation for a 2-panel pendulum oscillating in constant gravity field. . . . .	22
3.6	Satellite before array rotation. . . . .	23
3.7	Satellite after $90^\circ$ array symmetric rotation. . . . .	23
3.8	Satellite after $90^\circ$ array asymmetric rotation. . . . .	23
3.9	Angular momentum error for a sample internal torque reorientation trajectory of an array of three interconnected panels (L-shape) moving in vacuum. . . . .	24
3.10	Situation of no-collision for an array of 3 rods of equal length. . . . .	27
3.11	Situation of collision for an array of 3 rods of equal length. . . . .	27
4.1	Initial (dashed) and final (solid) states of the 3-rod planar array for a sample <i>rest-to-rest</i> and <i>flat-to-flat</i> reorientation manoeuvre. . . . .	30
4.2	Comparison of optimal control effort trajectories correcting $\Delta\theta=10^\circ$ in $t_M=25$ s (dashed in Sub-figures (a,b)) and $t_M=50$ s (solid in Sub-figures (a,b)). Dashed in Sub-figures (c,d,e,f) indicates the initial configuration of the rods which follow the same reorientation path in both cases. . . . .	30
4.3	Comparison of minimum time trajectories correcting $\Delta\theta=70^\circ$ with (solid in Sub-figures (a,b)) and without (dashed in Sub-figures (a,b)) impingement avoidance constraint. Dashed in Sub-figures (c,d,e,f) indicates the initial configuration of the rods which follow the same reorientation path for both cases. . . . .	32
4.4	Clockwise rectangular <i>flat-to-flat</i> reorientation manoeuvre. . . . .	33

4.5	Variation of $\theta_a$ as a function of $\psi_1$ for different lock angle positions $\psi_{2,lock}$ and $b_5 = 0$ . . . . .	35
4.6	Shape angle <i>flat-to-flat</i> manoeuvre for $N < 3$ array achieving no reorientation. . . . .	35
4.7	Net reorientation for different <i>flat-to-flat</i> clockwise rectangular manoeuvres. The red prisms contain those shape-angles configurations of the reference system that are not feasible due to rods impingement. . . . .	36
4.8	L-shape array performing a 3D <i>flat-to-flat</i> rectangular reorientation manoeuvre. . . . .	37
4.9	L-shape multipanel system non-holonomic turn direction and efficiency. . . . .	38
4.10	L-shape multipanel system non-holonomic turn efficiency as a function of shape angle variation. . . . .	38
4.11	Multipanel system body axes directions after non-holonomic turns (X-axis is blue, Y-axis is red, Z-axis is green). . . . .	39

# List of Acronyms

ACS	Attitude Control System
COM	Centre Of Mass
DOF	Degrees Of Freedom
EOM	Equations Of Motion
GG	Gravity Gradient
GNC	Guidance Navigation and Control
IC	Initial Conditions
LEO	Low Earth Orbit
MSc	Master of Science
MSL	Mars Science Laboratory
PID	Proportional Integral Derivative
PD	Proportional Derivative
SRP	Solar Radiation Pressure



# 1 Introduction

In the last few years interest in versatile reconfigurable arrays for space applications has been growing and several concepts tailored for different mission needs have been proposed [1, 2, 3]. Nevertheless, a compelling application that justifies their higher cost and complexity with respect to conventional systems has not yet been found. Here a novel approach to the design of an Attitude Control System (ACS) for small reconfigurable spacecraft is proposed. It shall exploit momentum-preserving internal torques generated by the modules of a multibody array rotating relative to each other. The end goal is to achieve better performance in efficiency, accuracy and robustness with respect to state-of-the-art ACS, which is a bottleneck for small spacecraft technology [4].

## 1.1 The Reconfigurable Spacecraft

A system is said to be reconfigurable if it can adapt its configuration to different situations and comply with the requirements of a certain number of operational needs. Reconfigurable arrays represent the state of the art in robotics technology, closely related to advanced nonlinear control and artificial intelligence. According to the definition of [5], *“self-reconfiguring robots are able to deliberately change their own shape by rearranging the connectivity of their parts, in order to adapt to new circumstances, perform new tasks, or recover from damage”*, and so can potentially be employed for more than one task.

In [5] it is also suggested that space engineering could represent a technological field where it is possible to consider a number of applications that would benefit from the advantages that autonomous reconfigurable arrays offer. Spacecraft whose solar panels remain folded during the launch phase and are deployed to maximise the area exposed to the Sun once released into orbit and robotic manipulators are examples of already existing reconfigurable space systems. In the last few years the research effort for the development of new classes of reconfigurable arrays, such as formation-flying systems, has been growing. An interesting concept, presented by [6] and further developed by [7], is a batch of cubic modules linked by means of temporary electromagnetically-actuated hinges. The shape of the array can be modified by sequentially creating and breaking these interconnections between the cubes. Other examples are self-

assembling [8] and self-folding origami structures [9].

Despite the advantages reconfigurable arrays offer over fixed-configuration systems and the impressive technological growth they have been recently experiencing, many challenges to their commercial exploitation still have to be overcome. One obstacle is to find specific compelling applications that justify the increase in overall system complexity and theoretical lower performance in single tasks compared to the gain in versatility they could guarantee. Also, as again suggested by [6], “*spacecraft reconfiguration technologies have not matured yet to the point in which they can be considered robust*”, this being a driving requirement for every space system.

Another research field that has been increasingly drawing attention and investments over recent years is that of small satellites. These systems, that today are mostly used for Earth Observation and Low Earth Orbit (LEO) communications, are cheaper and have shorter development times with respect to large satellites [10]. They are used by universities for educational purposes, commercial stakeholders seeking low-risk missions and technology demonstration opportunities or other applications requiring prompt deployment. Also, small satellites are more suitable for serving as modules of distributed space systems such as formations, which may be a crucial technology for the future.

As suggested by [11], however, “*cheap and light, implies a lot of compromises not only on the operational side but also on the design, the reliability and the lifetime*”. The reason is that today small spacecraft can be equipped with the latest technologies but these are not always space qualified. Also, small spacecraft “*will always be limited by their capacity to carry a payload and to supply it with the required power*” and are still outperformed by large spacecraft in terms of ACS performance. As a result, small satellite missions are often considered complimentary and not competitive to large satellite missions. The latter represents indeed the most appropriate choice when high reliability, functional flexibility, pointing accuracy or high payload power supply are key requirements.

According to [4], ACS for small satellites are still in an early development phase and represent a bottleneck for their technology, especially from the points of view of dynamic control and accuracy. The result is that current systems cannot satisfy stringent requirements for tasks including precise remote sensing. It is clear then that consistent improvements of the ACS subsystem would allow for their employment in high performance missions and pave the way for the commercial development of a novel class of space arrays that can compete with large satellites in a wider variety of market sectors.

An ingenious solution to the issues introduced by this analysis could be the redefinition of the architecture of small spacecraft so that the reconfiguration capability is used not only for complying with the requirements of different mission phases, but also actively for attitude control purposes. In particular, the idea is to exploit the effect of momentum-preserving internal torques that are generated by the elements of a modular spacecraft rotating with respect to each other. These dynamic contributions in fact have an indirect influence on the absolute orientation of the array and of the single modules themselves. The reference spacecraft we wish

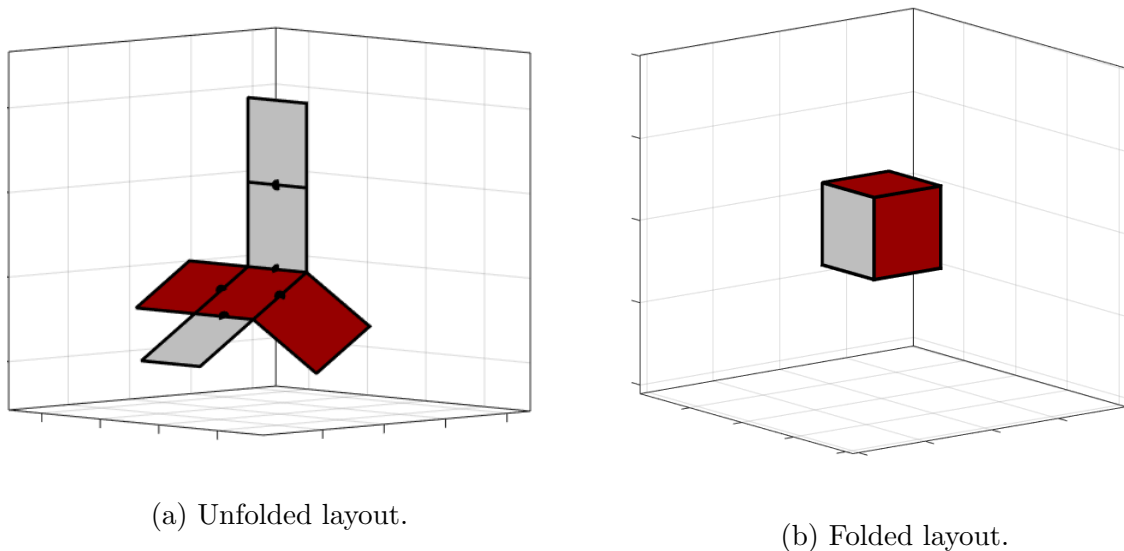


Figure 1.1: Multipanel cubic spacecraft.

to control, whose layout is given in Fig. 1.1, consists of rigid panels to which instrumentation, solar cells or other subsystems can be attached, interconnected using robust revolute joints. The research objective is to evaluate the potential of an innovative approach to the design of ACS for small spacecraft in which the configuration of the array, i.e., the relative position and relative motion of its modular components, become active players in the control of the attitude of the system in space.

## 1.2 Internal Torques for Attitude Control

The well-known *falling-cat problem* [12] represents the base of the idea introduced. Its physical explanation demonstrates the possibility, under certain conditions, to obtain absolute reorientation by exclusively using momentum-preserving internal torque contributions. Examples of this concept relevant for our case include the study of [2], that determine optimal 3D reorientation trajectories for a three panel array in an L-shape, and [1, 13], which instead focus on the design of a planning algorithm that is able to build a reorientation trajectory by patching together a certain number of motion primitives taken from a database obtained by numerical simulation. This algorithm is also developed for the L-shape three panel array but then it is adapted and tested on a system with a larger number of interconnected panels.

A long-term development of this novel approach could justify the increase in cost and complexity of the reconfigurable array with advantages in the added versatility of the entire system that is able to fold, unfold and in general tune the orientation of its panels singularly according to pointing, thermal, structural and other subsystem requirements. It could additionally allow for better performance in ACS efficiency, accuracy, stability and even robustness, if appropriate failure mitigation and recovery strategies based on module reconfiguration are developed.

This thesis represents the first building block to reach the final goal of an autonomous, intelligent reconfigurable spacecraft. Here the focus is to understand what is the characteristic behaviour of a multibody system rotating in free space when it is subjected to momentum-preserving internal torques and how these can be exploited for attitude control. As explained in Chapter 2, the analysis will first be conducted on a planar array that is an approximation of the multipanel spacecraft of Fig. 1.1 and recalls the dynamical properties that are relevant for the purpose of the study. As shown later in Fig. 2.3, the simplified system is a chain of three rods and its three rotational Degrees Of Freedom (DOF) are to be controlled with only two internal joint torques, which makes its full attitude stabilization fall in the class of *underactuated* control problems. These problems are characterised by complex dynamics due to dominating nonlinearities and are most often treated by means of numerical and artificial intelligence techniques, especially in the field of advanced robotics.

The determination of a control scheme for the orientation of a planar system of three rods only using two internal torques is a representative problem in its field that has already been analysed by several authors. The results obtained for it are indeed also valid for analogous chains which count  $N > 3$  modules since these can always be reduced to  $N = 3$  by locking some hinges. Also, as stated by [3], a simpler planar system with  $N = 2$  does not satisfy the mathematical condition of (*small time*) *local controllability*. This is the ability of a control system to reach a definite state from a fixed initial state in a (small) finite amount of time and is necessary for the internal torque reorientation problem to be solved. Interesting data were derived from the analytical study of *rest-to-rest* manoeuvres. Reyhanoglu and McClamroch [3, 14, 15] prove that smooth feedback control of the three rod planar arrays is impossible and derive an explicit non-smooth mathematical scheme for the system to reach a chosen equilibrium configuration. Walsh and Sastry [16] tested an analogous law on a lab prototype of the three rod system and adapted it for controlling the attitude of a satellite with two rotors. Finally, [17] and [18] analyse in general how to control the configuration and attitude of classes of planar multibody systems with  $N$  modules.

After proving the validity of the concept with the planar system the focus will be moved to a 3D multipanel array analogous to the one in Figure 1.1. The increase in mechanical complexity will result in more extended reorientation possibilities and a deeper understanding of the use of internal torques for attitude control in real applications. It is remarked that the focus is on the reorientation of the spacecraft as a whole and not on relative pointing of the single modules.

### 1.3 Thesis Overview

The primary objective of this thesis is to investigate the characteristic behaviour of planar and non-planar multibody arrays whose attitude is controlled using internal joint torques. To do this, first a multibody formalism is introduced and adapted to the specific needs of the research and then this is applied for the development of 2D and 3D simulation tools that, after

validation, can be used for analysing the peculiar dynamic behaviour of this class of under-actuated systems. The development of these tools represents the secondary objective of this work.

The multibody behaviour analysis, that shall serve the achievement of the primary objective, is done by discussing relevant reorientation trajectories generated using the tools developed in fulfillment of the secondary objective. With respect to previous work on the topic, this thesis adds the analysis of optimal reorientation trajectories for which impingement constraint avoidance is enforced and, importantly, explains in detail the mechanics, planar and non-planar, of momentum-preserving reorientation manoeuvres from both physical and mathematical points of view.

Starting by studying the behaviour of a simpler array, whose mechanics can be related to that of the system in Figure 1.1, is the most efficient choice for this purpose. Chapter 2 introduces the mathematical/physical background and multibody formalisms which is adapted and exploited for defining the reference models to be simulated. In particular, Section 2.2 describes the planar multibody array, while the modelling of the multipanel array in 3D is the core of Section 2.3. Both the developed planar and 3D multibody simulation tools have been validated. The test campaign is the main topic of Chapter 3, where also other resources used for this study are presented. In Chapter 4 the motion of the arrays is simulated and their dynamical behaviour is discussed. Chapter 5 concludes the study and suggests the next steps.

## 1.4 Published work

The present thesis describes in detail the tools developed and the corresponding validation process that have been used for obtaining the results published in:

Trovarelli, F., McRobb, M., Hu, Z., and McInnes, C. (2020)

*Attitude Control of an Underactuated Planar Multibody System Using Momentum Preserving Internal Torques*. AIAA Scitech 2020 Forum, AIAA 2020-1686, DOI:10.2514/6.2020-1686.

and extends these to more complex 3D systems, paving the way to further developments in the field.

## 2 Mechanics Background

Newton's laws of motion are the starting point for determining the EOM of any dynamic system. Nevertheless, they only hold for an inertial reference frame. In flight dynamics or multibody modelling applications, however, several non-inertial frames are commonly used, for example for defining the inertia of a body with respect to a local reference frame fixed to its centre of mass. When defining the dynamics of a mechanical system it is important that all vectors and matrices are defined with respect to same reference frame and because of this sometimes frame transformations are necessary. In addition to this, when interconnected bodies move relative to each other, apparent and internal torques have to be defined. This Chapter is dedicated to these topics. In Section 2.1 the tools that are used for representing the position and attitude of a body and how to transform from one reference to another are discussed. Then in Sections 2.2 and 2.3 the chosen multibody formalism is described and applied for the definition of the planar and 3D multibody models that will be exploited in the following Chapters for obtaining the desired results.

### 2.1 Reference Frames & Transformations

A reference frame consists of a set of three mutually orthogonal axes that intersect in the origin of the frame. For the purpose of studying the dynamics of a flying vehicle, many reference frames, either inertial or non-inertial, can be used. Frame transformations are possible if the relative position and orientation of a frame with respect to another, namely the state and attitude of the vehicle, is known. For identifying the spacecraft position and velocity several sets of variables can efficiently be adopted. In our case we will use *cartesian components* that identify the position with the elements  $x, y, z$  and the velocity with  $\dot{x}, \dot{y}, \dot{z}$ .

On the other hand, the attitude of a vehicle can be determined using the sets of *Euler angles*, namely the roll angle  $\phi$ , the pitch angle  $\theta$  and the yaw angle  $\psi$ , that determine the attitude of the body with respect to a chosen inertial frame or a local horizontal plane. When using these angles it is important to determine the sequence of rotations that realizes the transformation. For aerospace applications the most commonly used sequence is the 3-2-1, consisting of a yaw rotation about the  $Z$ -axis followed by pitch and roll rotations around, respectively, the local  $Y$ - and  $X$ -axes, as shown in Fig. 2.1.

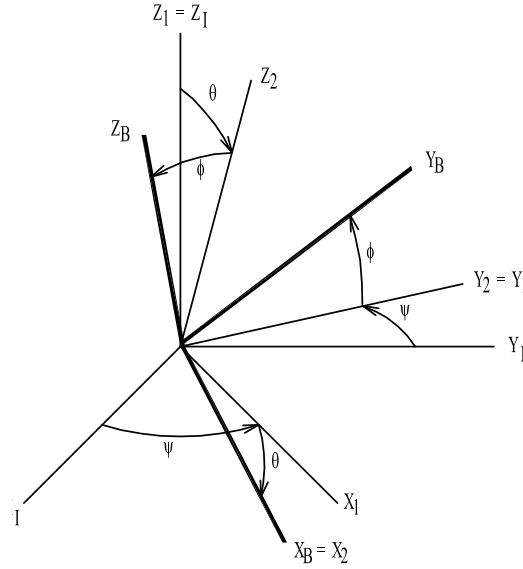


Figure 2.1: Classical angles  $\theta$ ,  $\phi$ ,  $\psi$  relating body  $B$ - and inertial  $I$ -frames [19] [used with permission].

Another attitude representation is the Euler axis–angle set. In this case the attitude or rotation is represented by a rotation axis  $\mathbf{a}$  and a rotation angle  $\phi$  around it for a total of 4 elements. The axis–angle representation is convenient when dealing with rigid body dynamics. It is useful to both characterize rotations, and also for converting between different representations of rigid body motion, such as homogeneous transformations.

For better numerical efficiency in 3D dynamic simulations, *quaternions* are the best solution because are not affected by the singularities that characterize Euler angles. Quaternions are 4-dimensional hyper-complex vectors consisting of one real number, the scalar part, and three imaginary numbers, the vector part. The imaginary numbers are square roots of -1 and are linked through the constraint:

$$i^2 = j^2 = k^2 = ijk = -1 \quad (2.1)$$

A quaternion can be defined in terms of the Euler axis  $\mathbf{a}$  and Euler angle  $\phi$ . The scalar and vector part are respectively:

$$q_0 = \cos \frac{\phi}{2} \quad (2.2)$$

$$\mathbf{q} = \begin{bmatrix} q_1 \\ q_2 \\ q_3 \end{bmatrix} \sin \frac{\phi}{2} \quad (2.3)$$

Attitude quaternions specify a rotation and have to satisfy the normality constraint:

$$q_0 + \mathbf{q}^T \mathbf{q} = q_0 + q_1 + q_2 + q_3 = 1 \quad (2.4)$$

Finally, we need to define the angular rate of the body that is defined as the rotational velocity of the body frame with respect to the chosen inertial frame, expressed in components along the body axes. The angular rate vector  $\boldsymbol{\omega}$  contains the roll rate  $p$ , the pitch rate  $q$  and the yaw

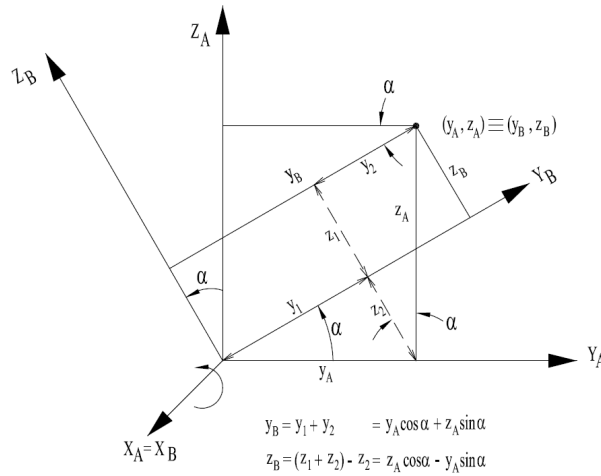


Figure 2.2: Reference frame transformation from **A** to **B** [19] [used with permission].

rate  $r$ . Any frame transformation can be written as the sum of a translation and a rotation. As suggested by Fig. 2.2, to express the vector  $\mathbf{v}_A$  in the **A** frame with respect to the **B** frame we write:

$$\mathbf{v}_B = \mathbf{T} + \mathbf{C}_{B,A} \mathbf{v}_A \quad (2.5)$$

where  $\mathbf{T}$  is the translation vector that goes from the origin of the **A** frame  $\mathbf{O}_A$  to the origin of the **B** frame  $\mathbf{O}_B$  and  $\mathbf{C}_{B,A}$  is the rotation matrix from frame **A** to frame **B** given by [19]:

$$\mathbf{C}_{B,A} = \begin{bmatrix} 1 & 0 & 0 \\ 0 & \cos \alpha & \sin \alpha \\ 0 & -\sin \alpha & \cos \alpha \end{bmatrix} \quad (2.6)$$

This orthonormal matrix, as suggested in Fig. 2.2, can be derived by expressing the components of the vector  $\mathbf{v}_A$ , defined with respect to the axes of the **A** frame, with respect to the axes of the **B** frame. More generally, if identified with the notation  $\mathbf{C}_1(\alpha)$ , the matrix in Eq. (2.6) gives the counter-clockwise rotation of a frame around its  $X$ -axis of a generic angle  $\alpha$ . Analogous expressions hold for the rotations around the  $Y$ - and  $Z$ - axes. We have respectively:

$$\mathbf{C}_2(\alpha) = \begin{bmatrix} \cos \alpha & 0 & -\sin \alpha \\ 0 & 1 & 0 \\ \sin \alpha & 0 & \cos \alpha \end{bmatrix} \quad (2.7)$$

$$\mathbf{C}_3(\alpha) = \begin{bmatrix} \cos \alpha & \sin \alpha & 0 \\ -\sin \alpha & \cos \alpha & 0 \\ 0 & 0 & 1 \end{bmatrix} \quad (2.8)$$

Also, a frame rotation can always be decomposed in a sequence of three rotations each around one of its independent axes. The resulting transformation matrix, that is still orthonormal, is found as the product of the three matrices  $\mathbf{C}_1$ ,  $\mathbf{C}_2$  and  $\mathbf{C}_3$ . Moreover, if  $\mathbf{C}_{B,A}$  is the matrix transforming frame **A** into frame **B**, then the opposite transformation, thanks to the fact that

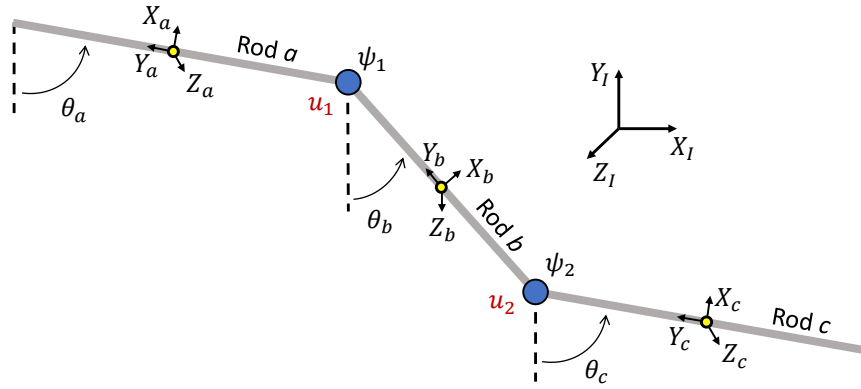


Figure 2.3: Planar array of 3 interconnected rods (Z-axes pointing out-of-plane).

rotation matrices are orthonormal, is given by the transpose:

$$\mathbf{C}_{\mathbf{A},\mathbf{B}} = \mathbf{C}_{\mathbf{B},\mathbf{A}}^{-1} = \mathbf{C}_{\mathbf{B},\mathbf{A}}^T \quad (2.9)$$

In cases when one is dealing with 2D vectors in a plane, then the rotation matrix can be reduced to size  $[2 \times 2]$ . In fact every 2D rotation can be described using a single angle and the row and column corresponding to the rotation axis (the one with only one term different from zero) is not needed any more. As for the 3D case the right hand rule determines the sign of the elements in the rotation matrix and the frame rotation direction can be counter-clockwise (as the one given by Eq. (2.6)) or clockwise.

Quaternions describe a sphere in 4-dimensions. Any quaternion rotation is a trajectory on this sphere. The quaternions  $[q_0 \ \mathbf{q}]$  and  $[-q_0 \ -\mathbf{q}]$  indicate the same orientation but correspond to paths with different length on the sphere. Transforming a vector given in frame  $\mathbf{A}$  to frame  $\mathbf{B}$  then can also be done using quaternions. The rotation process in this case is called quaternion multiplication. In general, the topic of quaternions is vast and will not be covered here, but more details will be discussed in the following when quaternions are applied.

## 2.2 Planar Multibody Mechanics

The most simple subset of the array in Fig. 1.1, to which internal torques can be successfully applied for attitude control purposes and that can yield relevant information, is the chain of three panels highlighted in red interconnected by two revolute joints. The array rotates in vacuum around its Centre Of Mass (COM), in absence of gravity or any other external disturbance. It is assumed that panels have uniform density and that their COMs always lie on the same common plane, perpendicular to the rotation axes of the frictionless revolute joints. As a result the rotation of the system is constrained to this plane. In consideration of this, without loss of generality with respect to the objectives of the thesis, we can study the equivalent planar system of three interconnected rods given in Fig. 2.3 rotating around its COM.

Internal joint torques only redistribute angular momentum among the modules and cannot be used for manoeuvres such as detumbling. The attitude control trajectories that will be analysed in the following describe *rest-to-rest* reorientation procedures that start and end in a condition where all the rods are stationary in space. The total angular momentum is always null. The objective is to obtain a variation in the net absolute orientation of the modules at the end of the manoeuvre by exclusively using internal joint torques which cause the shape of the array to change.

The equations of motion for the three-rod array are determined and propagated using the approach in Ref. [20] which is based on Lagrangian dynamics [21]. Each of its rigid elements, considered singularly, has one rotational and two translational DOF for a total of 9 DOF for the whole set of 3 rigid elements unconstrained with respect to each other or any external body. To get a multibody system the constraints that relate these rigid single elements have to be defined. The first constraint to take into account fixes the COM of the multibody to the origin of the inertial frame  $I$  and removes two translational DOF, so the following holds:

$$C_1 : \frac{m_a \mathbf{R}_a + m_b \mathbf{R}_b + m_c \mathbf{R}_c}{m_a + m_b + m_c} = \mathbf{0} \quad (2.10)$$

where  $\mathbf{R}_k = [x_k, y_k]$  is the position of the COM of rod  $k = a, b, c$  in the  $I$  frame and  $m_k$  is the corresponding inertial mass as shown in Fig. 2.3. Two other constraints model the revolute joints connecting the rods such that:

$$C_2 : \mathbf{R}_a + \mathbf{A}_a \mathbf{l}_{1a} - \mathbf{R}_b - \mathbf{A}_b \mathbf{l}_{1b} = 0 \quad (2.11)$$

$$C_3 : \mathbf{R}_b + \mathbf{A}_b \mathbf{l}_{2b} - \mathbf{R}_c - \mathbf{A}_c \mathbf{l}_{2c} = 0 \quad (2.12)$$

in which  $\mathbf{A}_i$  are the rotation matrices expressing the orientation of the rods and  $\mathbf{l}_{jk}$ , where  $k = 1, 2$  is the position of hinge  $j$  with respect to the COM of rod  $k$ .  $C_2$  and  $C_3$  also remove two translational DOF each. The multibody system, as modelled, is left with only three rotational DOF that, as already mentioned, can be controlled with only two inputs, the joint torques  $u_1$  and  $u_2$ . The state of the multibody system is described by a set of generalised coordinates  $\mathbf{q}$ . These can be subdivided in a group of independent coordinates  $\mathbf{q}_i$ , whose value can be chosen freely, and a group of dependent coordinates  $\mathbf{q}_d$ , which are a function of the independent coordinates through the constraint equations. The number of independent coordinates for the three rod array is  $n_i = 3$  and corresponds to the number of DOF of the system. The number of dependent coordinates  $n_d$  instead is equal to the number of available constraints. One can add an arbitrary number of dependent coordinates as long as these can be linked to the independent coordinates by means of some mathematical relationship.

The independent coordinates that will be used for our case are the orientation of rod  $a$ ,  $\theta_a$ , defined as the angle between the inertial frame reference axis negative  $Y_I$  and the direction of rod  $a$  (see Fig. 2.3), and the relative angles  $\psi_1$  and  $\psi_2$  determining the shape of the array given

by<sup>1</sup>:

$$C_4 : \quad \psi_1 = \theta_b - \theta_a \quad (2.13)$$

$$C_5 : \quad \psi_2 = \theta_c - \theta_b \quad (2.14)$$

Both Eqs. (2.13) and (2.14) have to be included together with Eqs. (2.10), (2.11), and (2.12) in the constraint vector  $\mathbf{C}$ . The sets of generalised coordinates are then  $\mathbf{q}_i = [\theta_a, \psi_1, \psi_2]$  and  $\mathbf{q}_d = [\theta_b, \theta_c, x_a, y_a, x_b, y_b, x_c, y_c]$ . When using the multibody methodology of [20] only the generalised independent accelerations  $\ddot{\mathbf{q}}_i$ , whose full general derivation and specific application both follow below, are directly defined as a function of the inertia of the array and the forces and torques acting on it and then integrated twice in time to get  $\mathbf{q}_i$ . In the classical Newtonian form we have:

$$\ddot{\mathbf{q}}_i = \mathbf{M}_i^{-1} \mathbf{Q}_i \quad (2.15)$$

where  $\mathbf{Q}_i$  and  $\mathbf{M}_i$  are respectively the generalised force vector and mass inertia matrix with respect to the independent coordinates. The generalised force vector  $\mathbf{Q}_i$  can be broken into 3 main terms. The Coriolis and gyroscopic inertia forces are taken into account by means of the vector  $\mathbf{Q}_v$ . These forces, however, are null for our case because the array is planar.  $\mathbf{Q}$  represents instead the explicit external and internal forces and torques contributions. It is remarked that all forces and torques contributions are decomposed with respect to the generalised coordinates  $\mathbf{q}$ . The order for listing them in  $\mathbf{Q}$  is fundamental and has to be the same as specified by the vector  $\mathbf{q}$ . This is valid also for the other vectors and matrices that are being defined. Since the only explicit contributions are the joint torques  $u_1$  and  $u_2$  directly acting on the shape angles  $\psi_1$  and  $\psi_2$ , for the three rod planar system described, in absence of external disturbances, the  $\mathbf{Q}$  vector is built as:

$$\mathbf{Q} = [0 \ u_1 \ u_2 \ 0 \ 0 \ 0 \ 0 \ 0 \ 0 \ 0 \ 0]^T \quad (2.16)$$

Finally,  $\bar{\mathbf{Q}}_c$  is defined as the vector that is used for taking into account the dynamic contributions due to the variation of the constraint matrix  $\mathbf{C}$  with respect to time [21]:

$$\bar{\mathbf{Q}}_c = \begin{bmatrix} \mathbf{0}_{[n_i \times 1]} \\ \mathbf{C}_{\mathbf{q}_d}^{-1} \mathbf{Q}_c \end{bmatrix}, \quad \mathbf{Q}_c = -\frac{\partial^2 \mathbf{C}}{\partial t^2} - \frac{\partial (\mathbf{C}_{\mathbf{q}} \dot{\mathbf{q}})}{\partial \mathbf{q}} - 2 \frac{\partial \mathbf{C}_{\mathbf{q}}}{\partial t} \quad (2.17)$$

where in  $\mathbf{Q}_c$  the first and last terms are null for the three rod array. In consideration of this,  $\mathbf{Q}_i$  can be written as:

$$\mathbf{Q}_i = \mathbf{B}_{di}^T (\mathbf{Q} + \mathbf{Q}_v) - \mathbf{B}_{di}^T \mathbf{M} \bar{\mathbf{Q}}_c \quad (2.18)$$

in which  $\mathbf{B}_{di}$  is by definition a matrix that expresses the virtual displacement of the dependent

---

<sup>1</sup>Note that the physical meaning of the results that will follow does not depend on which of the angles  $\theta_a$ ,  $\theta_b$  or  $\theta_c$  is chosen as a reference for the orientation of the array.

coordinates with respect to the independent coordinates and is defined as:

$$\mathbf{B}_{di} = \begin{bmatrix} \mathbf{I}_{n_i} \\ -\mathbf{C}_{\mathbf{q}_d}^{-1} \mathbf{C}_{\mathbf{q}_i} \end{bmatrix} \quad (2.19)$$

In Eq. (2.19)  $\mathbf{I}_{n_i}$  is the identity matrix of size  $n_i$  and  $\mathbf{C}_{\mathbf{q}_d}$  and  $\mathbf{C}_{\mathbf{q}_i}$  are derived from the Jacobian constraint matrix  $\mathbf{C}_{\mathbf{q}}$ :

$$\mathbf{C}_{\mathbf{q}} = \frac{\partial \mathbf{C}}{\partial \mathbf{q}}, \quad \mathbf{q} = [\mathbf{q}_i \ \mathbf{q}_d] \quad (2.20)$$

In particular,  $\mathbf{C}_{\mathbf{q}_i}$  is the left submatrix of  $\mathbf{C}_{\mathbf{q}}$  having its same number of rows and taking the first  $n_i$  columns while  $\mathbf{C}_{\mathbf{q}_d}$  is the remaining squared submatrix with size  $n_d$ . The generalised dependent coordinates  $\mathbf{q}_d$  can instead be propagated indirectly by integrating the generalised dependent velocities  $\dot{\mathbf{q}}_d$  which are expressed as a function of the generalised independent velocities  $\dot{\mathbf{q}}_i$  through the constraint equations [21]:

$$\dot{\mathbf{q}}_d = -\mathbf{C}_{\mathbf{q}_d}^{-1} \mathbf{C}_{\mathbf{q}_i} \dot{\mathbf{q}}_i \quad (2.21)$$

The generalised mass inertia matrix with respect to the independent coordinates  $\mathbf{M}_i$  in Eq. (2.15) is given by:

$$\mathbf{M}_i = \mathbf{B}_{di}^T \mathbf{M} \mathbf{B}_{di} \quad (2.22)$$

in which  $\mathbf{M}$  assuming that the origins of the body frames of the single rigid elements are placed at their respective COM, is a diagonal matrix. Similarly to the vector  $\mathbf{Q}$ , it contains the inertia terms of the body elements themselves that directly relate to the generalised coordinates, again arranged according to the order defined by  $\mathbf{q}$ . Since the mass/inertia terms corresponding to the relative shape angles are null, we have:

$$\mathbf{M} = \text{diag}(I_a, 0, 0, I_b, I_c, m_a, m_a, m_b, m_b, m_c, m_c) \quad (2.23)$$

with  $I_k$  being the moment of inertia of rod  $k$  around body axis  $Z_k$ . The rods, if not explicitly mentioned otherwise, are assumed to have a mass  $m_k$  of 1 kg and a half-length  $l_k$  of 1 m from which the corresponding moment of inertia can easily be calculated.

## 2.3 3D Multibody Mechanics

The 3D array mathematically described here is that depicted in Fig. 2.4. It is used as a reference for introducing the multibody modelling methodology and in the following simulations of Chapter 3 and 4. This L-shape mechanical system is particularly significant because it is the most simple multibody array consisting of equivalent panels that can rotate with respect to the 3 body-fixed axes of the reference panel (one of the three panels is selected as a reference for

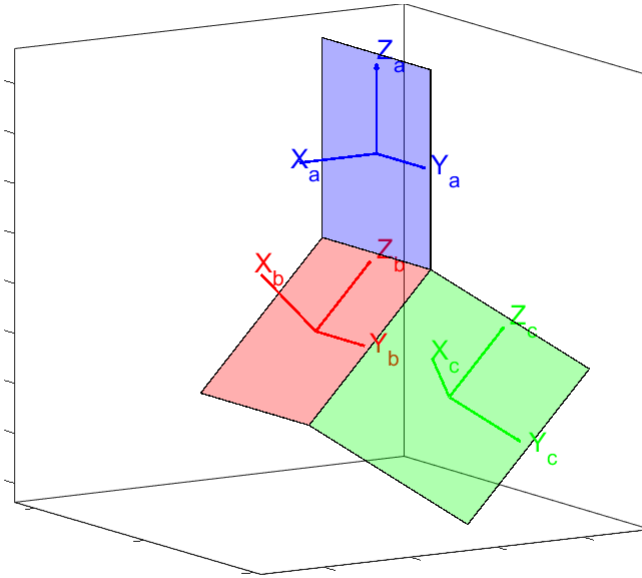


Figure 2.4: L-shape multipanel system with local reference frames.

calculating the absolute rotation of the whole array) by only exploiting internal torques in the hinges connecting the modules. As already suggested, a chain of equivalent panels would only rotate in one plane. The structure of the mechanical model is the same as for the planar case. The difference consists in the definition of several parameter matrices and vectors for taking into account cross-couplings of 3D rotational rates.

Each rigid body freely moving in 3D space features 3 translational and 3 rotational physical DOF. The state vector can be mathematically defined using different sets of variables that can eventually be more than 6. If this happens then it means that some of these variables are constrained between each other. A common approach is to use Cartesian variables  $[x, y, z]$  for defining the linear position of the COM of the body and quaternions  $[q_0, q_1, q_2, q_3]$  for its attitude, which gives a total of 7 state variables. In this case one of the quaternion elements is a function of the others through the quaternion constraint. For practical reasons we can subdivide between physical DOF and mathematical DOF. Physical DOF are related to the linear and rotational motion of the rigid body elements, are fixed to a maximum of 6 per each unconstrained rigid body and can be reduced if physical constraints are introduced in the mechanics. Mathematical DOF are not directly related to the motion of the rigid body elements and one can add as many mathematical DOF as desired as long as each of the corresponding mathematical variables depends on those already existing through some mathematical constraint function.

The unconstrained 3-body 3D array has a total of  $3 \times 6 = 18$  physical DOF. The state of each of the modules is defined by the variable set:

$$\mathbf{x}_k = [\mathbf{R}_k, \mathbf{q}_k] = [x_k, y_k, z_k, q_{0,k}, q_{1,k}, q_{2,k}, q_{3,k}] \quad (2.24)$$

where  $k = a, b, c$  is the panel index. Since there are 3 modules, at this point the system has 21 DOF of which 18 are physical and 3 are mathematical. The elements of the quaternion vector  $\mathbf{q}_k$  are mutually dependent due to the normal quaternion equation. This gives the first three

mathematical constraints:

$$C_1 : q_{0,a}^2 + q_{1,a}^2 + q_{2,a}^2 + q_{3,a}^2 = 1 \quad (2.25)$$

$$C_2 : q_{0,b}^2 + q_{1,b}^2 + q_{2,b}^2 + q_{3,b}^2 = 1 \quad (2.26)$$

$$C_3 : q_{0,c}^2 + q_{1,c}^2 + q_{2,c}^2 + q_{3,c}^2 = 1 \quad (2.27)$$

We now consider the physical constraints defining the dynamics of the system. Since the interest is exclusively in the array rotation, in this case we also fix its COM to the origin of an ideal inertial reference frame  $I$ :

$$C_4 : \frac{m_a \mathbf{R}_a + m_b \mathbf{R}_b + m_c \mathbf{R}_c}{m_a + m_b + m_c} = \mathbf{0} \quad (2.28)$$

where  $m_k$  is the corresponding inertial mass. Differently from  $C_1$ ,  $C_2$  and  $C_3$ , the constraint  $C_4$  is 3-dimensional and removes 3 physical DOF. The relative position of the COM of the panels are again constrained using the mathematical definition of the spherical articulation:

$$C_5 : \mathbf{R}_a + \mathbf{A}_a \mathbf{l}_{1a} - \mathbf{R}_b - \mathbf{A}_b \mathbf{l}_{1b} = \mathbf{0} \quad (2.29)$$

$$C_6 : \mathbf{R}_b + \mathbf{A}_b \mathbf{l}_{2b} - \mathbf{R}_c - \mathbf{A}_c \mathbf{l}_{2c} = \mathbf{0} \quad (2.30)$$

in which  $\mathbf{A}_i$  are the rotation matrices expressing the rotation from panel-fixed frames to the inertial frame  $I$  and  $\mathbf{l}_{jk}$ , where  $j = 1, 2$ , is the position of hinge  $j$  with respect to the COM of panel  $k$ . Also  $C_5$  and  $C_6$  remove 3 translational DOF each.

Now also the relative rotation of the panels has to be constrained. In particular, it is required that rotation is only possible around the axes defined by the hinges connecting them. This can be achieved using the panel normal vectors that are defined in panel fixed frames as:

$$\mathbf{X}_k = [1 \ 0 \ 0], \quad \mathbf{Y}_k = [0 \ 1 \ 0], \quad \mathbf{Z}_k = [0 \ 0 \ 1] \quad (2.31)$$

From Fig. 2.4 it is straightforward to understand that if panel  $b$  rotates only around the edge it shares with panel  $a$  then it means that its panel  $b$ -fixed body axes  $X_b$  and  $Z_b$  always remain perpendicular to panel  $a$ -fixed body axis  $Y_a$ . Mathematically this can be written as:

$$C_7 : \mathbf{Y}_a \cdot \mathbf{X}_b = \mathbf{A}_a \mathbf{Y} \cdot \mathbf{A}_b \mathbf{X} = 0 \quad (2.32)$$

$$C_8 : \mathbf{Y}_a \cdot \mathbf{Z}_b = \mathbf{A}_a \mathbf{Y} \cdot \mathbf{A}_b \mathbf{Z} = 0 \quad (2.33)$$

The same analysis for the rotation of panel  $c$  with respect to panel  $b$  leads to:

$$C_9 : \mathbf{Z}_a \cdot \mathbf{X}_c = \mathbf{A}_b \mathbf{Z} \cdot \mathbf{A}_c \mathbf{X} = 0 \quad (2.34)$$

$$C_{10} : \mathbf{Z}_a \cdot \mathbf{Y}_c = \mathbf{A}_b \mathbf{Z} \cdot \mathbf{A}_c \mathbf{Y} = 0 \quad (2.35)$$

By including constraints  $C_7$  to  $C_9$ , 5 additional physical DOF have been removed which leaves a system of only 5 DOF. Of these 5, 3 are for the rotation of the whole array in 3D space and

2 are for the relative rotations around the hinge axes. From a physical point of view this is the system which needs to be defined. From a mathematical perspective, however, there any set of variable can be used for describing the attitude state of the array. In particular, new variables can be introduced that are more suitable for the specific purpose of the model. Because of the requirement to control the attitude of the array using internal hinge torques, as a state variable the angle between two panels is introduced. This quantity, again by looking at the panel-fixed reference frames in Fig. 2.4, is defined as the angle between the normals to the panel surfaces. Mathematically this can be written as:

$$C_{11} : \alpha_{ba} = \sin^{-1}(\mathbf{A}_a \mathbf{X} \times \mathbf{A}_b \mathbf{X}) \quad (2.36)$$

$$C_{12} : \alpha_{cb} = \sin^{-1}(\mathbf{A}_b \mathbf{X} \times \mathbf{A}_c \mathbf{X}) \quad (2.37)$$

These generalised coordinates describe the state of the system defined by:

$$\mathbf{q} = \begin{bmatrix} x_a & y_a & z_a & q_{0a} & q_{1a} & q_{2a} & q_{3a} & \dots \\ x_b & y_b & z_b & q_{0b} & q_{1b} & q_{2b} & q_{3b} & \dots \\ x_c & y_c & z_c & q_{0c} & q_{1c} & q_{2c} & q_{3c} & \dots \\ \alpha_{ba} & \alpha_{cb} \end{bmatrix} \quad (2.38)$$

It is now required to select 5 that will be the set of independent generalised coordinates  $\mathbf{q}_i$  while the others will be the dependent generalised coordinates  $\mathbf{q}_d$ . This choice is suggested by the initial conditions to be specified when simulating the system and by the state variables that define our control strategy. For the specific case of interest an initial attitude of the array must be specified, for which one of the three quaternion sets can be chosen that give the orientation of the panels, and the shape of the array represented by the angles  $\alpha$ . Therefore, the vectors of generalised coordinates are given by:

$$\begin{aligned} \mathbf{q}_i &= [q_{1a} \quad q_{2a} \quad q_{3a} \quad \alpha_{ba} \quad \alpha_{cb}] \\ \mathbf{q}_d &= [q_{0a} \quad q_{0b} \quad q_{1b} \quad q_{2b} \quad q_{3b} \quad q_{0c} \quad q_{1c} \quad q_{2c} \quad q_{3c} \quad \dots \\ &\quad x_a \quad y_a \quad z_a \quad x_b \quad y_b \quad z_b \quad x_c \quad y_c \quad z_c] \end{aligned} \quad (2.39)$$

Then, the full generalised coordinate vector, that shall have first the independent and then the dependent coordinates, can be written as:

$$\mathbf{q} = [\mathbf{q}_i \quad \mathbf{q}_d] \quad (2.40)$$

The order in which the variables are reported in the vector of generalised coordinates plays a fundamental role in the definition of the equations of motion:

$$\ddot{\mathbf{q}}_i = \mathbf{M}_i^{-1} \mathbf{Q}_i \quad (2.41)$$

$$\dot{\mathbf{q}}_d = -\mathbf{C}_{\mathbf{q}_d}^{-1} \mathbf{C}_{\mathbf{q}_i} \dot{\mathbf{q}}_i \quad (2.42)$$

The process of determining the terms appearing in Eq. (2.15) and (2.42), which fully describe

in matrix form the dynamical contributions acting on the array, its geometry/inertia properties and kinematics, is analogous to that described in Section 2.2. Nevertheless, the increased complexity of 3D mechanical systems results in some relevant variations in the definition of these terms. First, in this case Coriolis and gyroscopic forces are not null because of cross-coupling of 3D rotational rates. We have for each of the rigid modules  $k$ :

$$\mathbf{F}_{C,k} = -2\boldsymbol{\omega}_k \mathbf{I}_k \dot{\mathbf{G}}_k \quad (2.43)$$

in which  $\boldsymbol{\omega}_k$  and  $\mathbf{I}_k$  are respectively the rotational rate and inertia tensor of body  $k$  both expressed in its corresponding local frame. The term  $\dot{\mathbf{G}}_k$  is instead the time derivative of the matrix that transforms attitude rotational rates, that are the quaternion elements time derivatives, to body rotational rates  $\boldsymbol{\omega}_k$ . The size and elements of this matrix depend on the choice of attitude representation used. For quaternions this can be written as:

$$\mathbf{G}_k = 2 \begin{bmatrix} -q_{1,k} & q_{0,k} & q_{3,k} & -q_{2,k} \\ -q_{2,k} & -q_{3,k} & q_{0,k} & q_{1,k} \\ -q_{3,k} & q_{2,k} & -q_{1,k} & q_{0,k} \end{bmatrix} \quad (2.44)$$

$$\dot{\mathbf{G}}_k = 2 \begin{bmatrix} -\dot{q}_{1,k} & \dot{q}_{0,k} & \dot{q}_{3,k} & -\dot{q}_{2,k} \\ -\dot{q}_{2,k} & -\dot{q}_{3,k} & \dot{q}_{0,k} & \dot{q}_{1,k} \\ -\dot{q}_{3,k} & \dot{q}_{2,k} & -\dot{q}_{1,k} & \dot{q}_{0,k} \end{bmatrix} \quad (2.45)$$

The rotational rate  $\boldsymbol{\omega}_k$  is then defined as:

$$\boldsymbol{\omega}_k = -2\mathbf{G}_k \dot{\mathbf{q}}_k \quad (2.46)$$

The apparent force dynamic contribution  $\mathbf{F}_{C,k}$  has size  $[1 \times 4]$ . Each of its elements expresses a dynamic contribution applied to the corresponding quaternion element, which is indicated by the superscript (1 corresponds to  $q_0$ , 2 to  $q_1$  and so on per each of the panels  $k$ ). Considering this and keeping in mind the generalised coordinates ordering chosen earlier in Eq. (2.39), the vector  $\mathbf{Q}_v$  of Coriolis and gyroscopic dynamic contributions can be defined for the system as:

$$\mathbf{Q}_v = \begin{bmatrix} \mathbf{F}_{C,a}^{\{2\}} & \mathbf{F}_{C,a}^{\{3\}} & \mathbf{F}_{C,a}^{\{4\}} & 0 & 0 & \dots \\ \mathbf{F}_{C,a}^{\{1\}} & \mathbf{F}_{C,b}^{\{1\}} & \mathbf{F}_{C,b}^{\{2\}} & \mathbf{F}_{C,b}^{\{3\}} & \mathbf{F}_{C,b}^{\{4\}} & \mathbf{F}_{C,c}^{\{1\}} & \mathbf{F}_{C,c}^{\{2\}} & \mathbf{F}_{C,c}^{\{3\}} & \mathbf{F}_{C,c}^{\{4\}} & \dots \\ 0 & 0 & 0 & 0 & 0 & 0 & 0 & 0 & 0 \end{bmatrix} \quad (2.47)$$

If the set of generalised coordinates uses quaternions then the definition of the mass-inertia matrix  $\mathbf{M}$  of the system has to be adjusted accordingly. In particular, first the inertia of each array needs to be defined with respect to the generalised coordinates that are selected. For each module  $k$  the mass-inertia matrix that relates to its physical DOF is defined as:

$$\mathbf{M}_k = \begin{bmatrix} \mathbf{m}_{RR,k} & \mathbf{m}_{R\theta,k} \\ \mathbf{m}_{R\theta,k} & \mathbf{m}_{\theta\theta,k} \end{bmatrix} \quad (2.48)$$

in which  $\mathbf{m}_{RR,k}$  is the sub-matrix containing the inertia terms that relate to the translational

DOF:

$$\mathbf{m}_{RR,k} = \begin{bmatrix} m_k & 0 & 0 \\ 0 & m_k & 0 \\ 0 & 0 & m_k \end{bmatrix} \quad (2.49)$$

with  $m_k$  being the mass of module  $k$ . The sub-matrix  $\mathbf{m}_{R\theta,k}$  represents the inertia coupling between the translation and rotation of the module and contains only 0 if the origin of the body axes is attached to the centre of mass of the module, which is assumed to be the case. Finally, the sub-matrix  $\mathbf{m}_{\theta\theta,k}$  is associated with the rotational DOF of the module and is defined as:

$$\mathbf{m}_{\theta\theta,k} = \mathbf{G}_k^T \mathbf{I}_k \mathbf{G}_k \quad (2.50)$$

and has size  $[4 \times 4]$  if quaternions are used. The mass-inertia matrix elements that relate to the mathematical DOF, that in this case are the two shape angles  $\alpha_{ba}$  and  $\alpha_{cb}$  are null. At this point the sub-matrices defined for each module  $k$  can be put together to get a single comprehensive mass-inertia matrix and rearrange its elements in agreement with the chosen order for the generalised coordinates vector. For this specific case  $\mathbf{M}$  is the diagonal block matrix (the superscripts indicate the specific elements selected in the matrices  $\mathbf{m}$  of the single elements defined earlier):

$$\mathbf{M} = \begin{bmatrix} \mathbf{m}_{\theta\theta,a}^{(2,2)} & \mathbf{m}_{\theta\theta,a}^{(2,3)} & \mathbf{m}_{\theta\theta,a}^{(2,4)} & 0 & 0 & \mathbf{m}_{\theta\theta,a}^{(2,1)} \\ \mathbf{m}_{\theta\theta,a}^{(3,2)} & \mathbf{m}_{\theta\theta,a}^{(3,3)} & \mathbf{m}_{\theta\theta,a}^{(3,4)} & 0 & 0 & \mathbf{m}_{\theta\theta,a}^{(3,1)} \\ \mathbf{m}_{\theta\theta,a}^{(4,2)} & \mathbf{m}_{\theta\theta,a}^{(4,3)} & \mathbf{m}_{\theta\theta,a}^{(4,4)} & 0 & 0 & \mathbf{m}_{\theta\theta,a}^{(4,1)} \\ 0 & 0 & 0 & 0 & 0 & 0 \\ 0 & 0 & 0 & 0 & 0 & 0 \\ \mathbf{m}_{\theta\theta,a}^{(1,2)} & \mathbf{m}_{\theta\theta,a}^{(1,3)} & \mathbf{m}_{\theta\theta,a}^{(1,4)} & 0 & 0 & \mathbf{m}_{\theta\theta,a}^{(1,1)} \\ & & & & & \mathbf{m}_{\theta\theta,b} \\ & & & & & \mathbf{m}_{\theta\theta,c} \\ & & & & & \mathbf{m}_{RR,a} \\ & & & & & \mathbf{m}_{RR,b} \\ & & & & & \mathbf{m}_{RR,c} \end{bmatrix} \quad (2.51)$$

which, analogously to the 2D case, has to be expressed in the reference of independent generalised coordinates  $\mathbf{q}_i$  using the transformation of Eq. (2.22).

The last term of the total force vector  $\mathbf{Q}_i$  expressed in the independent coordinate frame of Eq. (2.18) that must be defined is the vector  $\mathbf{Q}_e$ . This allows any external dynamic contributions acting on the system to be taken into account. Also in this case each element of this vector directly affects the generalised coordinate which occupies the equivalent position in the vector  $\mathbf{q}$ , that can be either independent and dependent. In the assumption that the system moves in vacuum and that the only available actuators for influencing its orientation are hinge motors

that control the shape angles  $\alpha_{ba}$  and  $\alpha_{cb}$  it is found that:

$$\mathbf{Q}_e = \begin{bmatrix} 0 & 0 & 0 & u_1 & u_2 & \dots & & & & & \\ 0 & 0 & 0 & 0 & 0 & 0 & 0 & 0 & 0 & 0 & \dots \\ 0 & 0 & 0 & 0 & 0 & 0 & 0 & 0 & 0 & 0 & 0 \end{bmatrix} \quad (2.52)$$

where  $u_1$  and  $u_2$  are the commanded hinge torques. Finally, it is important to calculate the total energy and total angular momentum of the system that can be used for monitoring its state and for model validation purposes for both the 3D and previous 2D cases. The former is the sum of rotational and translational energies of the system that can be found respectively as:

$$E_{\text{rot}} = \frac{1}{2} \begin{bmatrix} \dot{\mathbf{q}}_a & \dot{\mathbf{q}}_b & \dot{\mathbf{q}}_c \end{bmatrix} \begin{bmatrix} \mathbf{m}_{\theta\theta,a} & & \\ & \mathbf{m}_{\theta\theta,b} & \\ & & \mathbf{m}_{\theta\theta,c} \end{bmatrix} \begin{bmatrix} \dot{\mathbf{q}}_a & \dot{\mathbf{q}}_b & \dot{\mathbf{q}}_c \end{bmatrix}^T \quad (2.53)$$

$$E_{\text{tra}} = \frac{1}{2} \begin{bmatrix} \dot{\mathbf{R}}_a & \dot{\mathbf{R}}_b & \dot{\mathbf{R}}_c \end{bmatrix} \begin{bmatrix} \mathbf{m}_{\text{RR},a} & & \\ & \mathbf{m}_{\text{RR},b} & \\ & & \mathbf{m}_{\text{RR},c} \end{bmatrix} \begin{bmatrix} \dot{\mathbf{R}}_a & \dot{\mathbf{R}}_b & \dot{\mathbf{R}}_c \end{bmatrix}^T \quad (2.54)$$

For the latter, the angular momentum of each of the modules is defined as:

$$\mathbf{H}_k = \mathbf{I}_k \boldsymbol{\omega}_k \quad (2.55)$$

Then, these momenta have to be expressed with respect to a common reference and also the additional momenta due to the shift of reference have to be computed. The total angular momentum of the system then is:

$$\mathbf{H}_{\text{tot}} = \sum_k \mathbf{A}_k \mathbf{H}_k + \mathbf{R}_k \times m_k \dot{\mathbf{R}}_k \quad (2.56)$$

The multibody mechanical models presented in this Chapter is coded in MATLAB for simulation purposes. Chapter 3 validates these models by exploiting the output of available simulators tested, amongst others, with respect to the introduced definitions of system energy and total angular momentum which are particularly relevant for this class of systems.

# 3 Simulator Development

The present Chapter is dedicated to describing the simulator that implements the mechanics of the multibody systems introduced in the previous Chapter. For both the planar and 3D cases, first the mass and inertia properties are defined and then the validity of the simulation environment is validated with some significant tests. Some software aspects to take into account when designing a multibody simulator are discussed and finally the supporting tools that have been exploited for this thesis are introduced.

## 3.1 Planar Model Model Simulator

The objective of the model is to prove the validity of the internal torque control strategy. For this reason the absolute mass and inertia properties of the array that is simulated are not a primary concern as long they are relatively consistent with each other. Nevertheless, as a reference for the purpose of being able to reproduce the results the mass-geometry inertia parameters of the model implemented are reported here. Each equivalent rod is assumed to have a mass of  $m = 1$  [kg] and a length of  $l = 2$  [m]. The moment of inertia around the respective rotational axis passing through their COM, at the geometric centre of the rod, is:

$$I_k = \frac{ml^2}{12} \quad (3.1)$$

In the following Section the Validation & Verification process is described and then some relevant details related to the development of the multibody array simulation software that have to be taken into account when working with analogous systems are discussed.

### 3.1.1 Validation & Verification

For the purpose of testing its validity, this multibody design approach was used for building a triple pendulum system oscillating under the effect of Earth gravity. This model features minor modifications with respect to the three rod model presented earlier. It was verified that its total energy remains constant. Also it was checked that, for the spacecraft control problem, the total angular momentum for every attitude control manoeuvre not involving external dynamic

contributions always remains constant. In both cases an acceptable inaccuracy due to numerical propagation error, that reduces if more stringent integrator tolerances are selected, was present. This Validation & Verification process is not further described here because it is analogous to that for the 3D model discussed in the following Section 3.2.1 in much greater detail.

### 3.1.2 Implementation Aspects

In Section 4.1.2 the multi-rod planar model will be used to simulate so-called *rectangular trajectories*. These trajectories, that will be better explained later, require that the system has the ability to lock a certain hinge at an arbitrary instant in time. The array has been designed for being able to input desired hinge torques for controlling its attitude. While it is straightforward to define a hinge torque as a function of the shape angles using a proportional feedback control logic, there is not a law that allows us to determine the torque that applies to the hinge when one of these shape angles gets locked.

The solution that has been adopted for the planar model consists of assuming that when locked the hinge behaves as an extremely stiff rotational spring. In particular, the command sequence that is given in input to the simulator includes a flag for the activation of the locking mode. In this case the command torque is computed using a proportional-derivative law with very large gains. While this approach is physically consistent because every rigid body is elastic to some extent, simulating micro-oscillations is extremely computationally intensive. It was also verified that the approach does not violate the validity tests mentioned above, but when the locking takes place the numerical error experiences a discontinuity causing it to increase in magnitude. This increase also depends on the the integrator properties.

## 3.2 3D Model Simulator

As with the planar model, the objective of this model is to prove the validity of internal torque control strategy. Again, the absolute mass inertia properties of the array that is simulated are not a primary concern as long they are relatively consistent with each other. Nevertheless, as a reference for the purpose of being able to reproduce the results, the mass-geometry inertia parameters of the 3D model implemented are reported here. Each equivalent square panel is assumed to have a mass of  $m = 1$  [kg] and side length of  $l = 1$  [m]. Assuming that the panels are  $t = 0.01$  [m] thick, its moment of inertia relative to the reference frame fixed to its COM, which is located at the geometric centre of the panels as depicted in Fig. 2.4, can be found using the formula that applies for a cylindrical prism:

$$\mathbf{I}_k = \begin{bmatrix} \frac{m(l^2+t^2)}{12} & 0 & 0 \\ 0 & \frac{m(l^2+t^2)}{12} & 0 \\ 0 & 0 & \frac{m(l^2+t^2)}{12} \end{bmatrix} \quad (3.2)$$

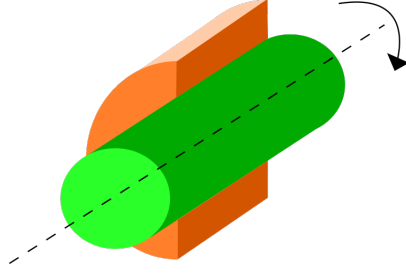


Figure 3.1: Typical revolute joint motion.

Again, in the following the Validation & Verification process is described and then some relevant details related to the development of the multibody array simulation software that have to be taken into account when working with analogous systems are discussed.

### 3.2.1 Validation & Verification

The Validation & Verification process for the 3D multibody modelling methodology presented in Section 2.3 was run in parallel with model development and was based on simulating multibody pendulums oscillating in a constant Earth gravity field. The first test consisted of analysing the motion of a single panel that is suspended through a spherical connection placed in the central point of one of its sides. This simple test showed that the rigid body oscillates as expected in the 3D space and thus verified that the equations of motion for the 3D case are correctly implemented.

The second test consisted of several steps. First, to the single panel moving under the effect of gravity a second panel was attached below by means of a revolute joint that only allows one degree of freedom between the two rigid elements. These rotate relatively only around their common side, i.e., the one connected through the revolute joint axis whose schematic is shown in Figure 3.1. In this case the oscillatory motion of the system was analysed more in depth. The focus was on the total energy of the system that, because of the fact that it moves in a conservative force field, shall remain constant. With respect to the study case of Section 2.3, in addition to rotational and translation kinetic energies computed using Eq. (2.54) and (2.53), for this specific validation case the gravitational potential has to be taken into account for calculating the total energy of the system. In the assumption that gravitational acceleration only has a component along the Z inertial direction, the gravitational potential energy can be determined as:

$$E_{\text{pot}} = \sum_k m_k g_0 R_{z,k} \quad (3.3)$$

where  $k$  is the rigid element index and  $g_0 = 9.81 \text{ [m/s}^2\text{]}$  is the Earth surface gravitational acceleration. Figure 3.2 shows conditions of the pendulum at  $t = 0\text{[s]}$  that is fixed to the

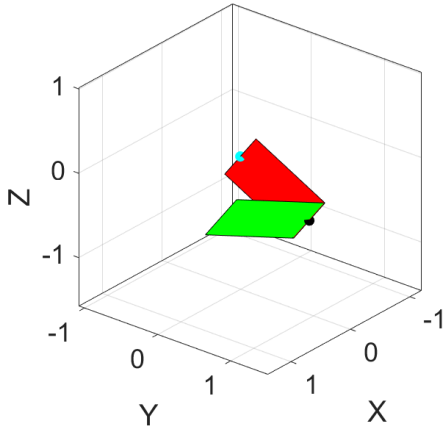


Figure 3.2: 2-panel pendulum in constant gravitational field, conditions at  $t = 0$  [s].

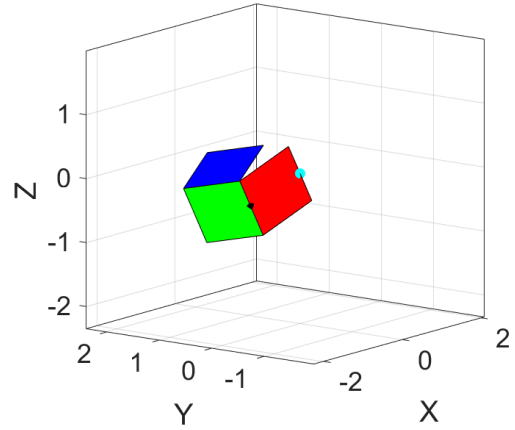


Figure 3.3: 3-panel pendulum in constant gravitational field, conditions at  $t = 0$  [s].

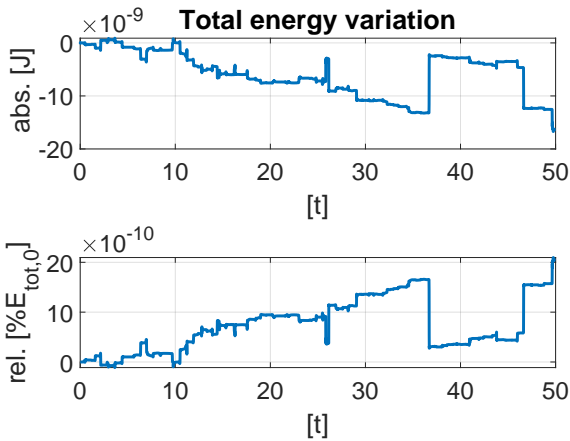


Figure 3.4: Total energy variation for a 2-panel pendulum oscillating in constant gravity field.

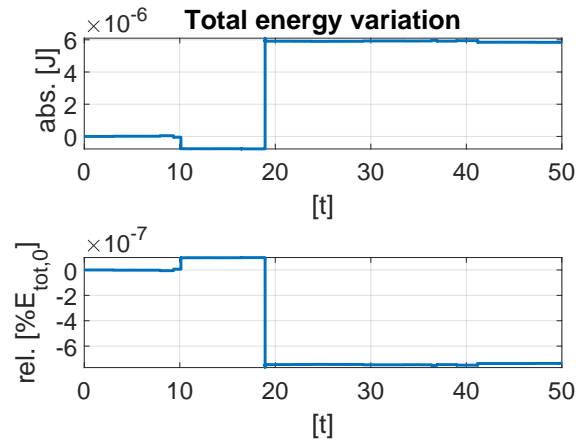


Figure 3.5: Total energy variation for a 2-panel pendulum oscillating in constant gravity field.

inertial frame only through the light blue hinge. Part of the potential energy that the pendulum has at this moment transforms to kinetic energy as soon as it starts oscillating. Nevertheless, Fig. 3.4 shows how the total energy, as expected, remains almost constant with respect to its initial value. The small variation, however, is not exactly zero as expected from theory because of numerical integration errors that accumulates during the simulation and reduces if more stringent integrator tolerances are used at the expense of a lower computational efficiency. This is especially true when dealing with complex systems whose dynamics are complex and requires matrix multiplication and inversions as for our case. This is confirmed by the fact that by running the same total energy test using the L-shape model of 3 panels, whose dynamics is defined by a larger number of constraints, the resulting propagation error was still compatible with what is expected from numerical propagation inaccuracy, but is some orders of magnitude larger than the error for the 2 panel model simulation, as Figure 3.5 confirms.

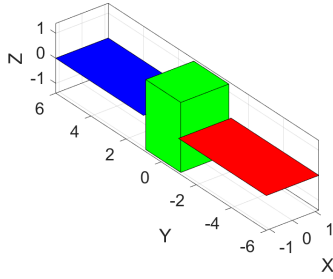


Figure 3.6: Satellite before array rotation.

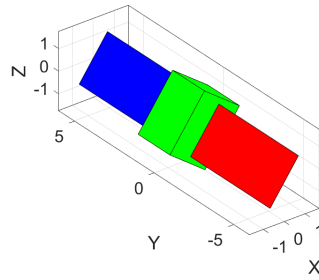


Figure 3.7: Satellite after  $90^\circ$  array symmetric rotation.

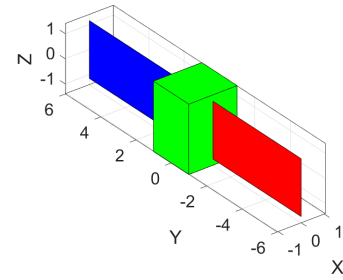


Figure 3.8: Satellite after  $90^\circ$  array asymmetric rotation.

Also in these two cases the sample oscillatory trajectories were analysed graphically and it was verified that the motion was consistent with what was physically expected. A graphical validation test was additionally run by designing the multibody system representing the dynamics of a spacecraft consisting of a central body with 2 solar arrays attached symmetrically on its sides moving in vacuum. By comparing Fig. 3.6, 3.7 and 3.8, it can be verified that when the equivalent solar arrays rotate about their respective longitudinal axes in the same direction with respect to the central block then the latter rotates in the opposite direction. If however the arrays rotate in opposite directions then they exert equal and opposite torques on the central block that remains fixed with respect to the inertial reference frame. This test additionally proves the flexibility of the multibody dynamics tool that can be adapted to any different system configuration.

This second test demonstrated that the revolute joint constraints, that are very prone to cause numerical errors, were implemented correctly and that the model behaviour was consistent with physical expectations.

The last and third test involved the analysis of the angular momentum of the multibody array moving in vacuum and controlled using exclusively internal torques whose mechanics was described in Section 2.3. Its angular momentum shall always remain constant irrespective of the internal torques applied to it. Figure 3.9 shows the variation of angular momentum for a sample internal torque reorientation trajectory. Also in this case the absolute variation is compatible with numerical propagation inaccuracy. The relative error had to be calculated using the final angular momentum because the initial angular momentum is null and is thus not significant for the test.

The success of this last test demonstrates that the integration of internal torques in the multibody dynamics is correct and the resulting simulation environment yields physically consistent results.

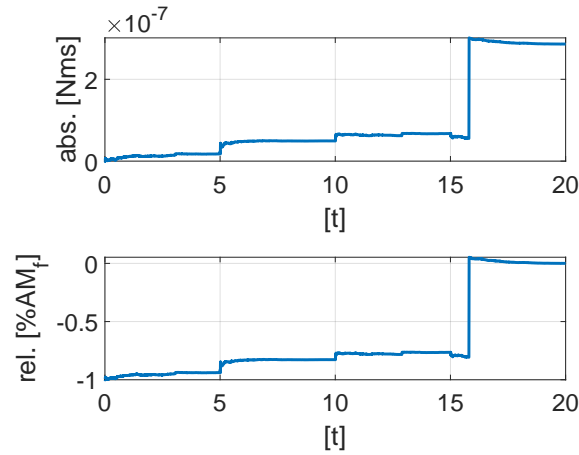


Figure 3.9: Angular momentum error for a sample internal torque reorientation trajectory of an array of three interconnected panels (L-shape) moving in vacuum.

### 3.2.2 Implementation Aspects

As already done for the planar multibody model, the system shall be able to simulate the locking of the hinge angles. Given the much larger number of variables and constraints involved in the definition of the hinge angles for the 3D multipanel case, the approach of implementing locking by means of the stiff spring method is not applicable since it causes significant numerical instability and dramatically reduces computational efficiency. The alternative solution that was implemented to solve this issue consists of first substituting the two shape angles  $\alpha_{ba}$  and  $\alpha_{cb}$  with  $\alpha_{lock}$  and  $\alpha_{free}$ . Second, the constraint

$$\alpha_{lock} = \alpha_{lock}^* \quad (3.4)$$

where  $\alpha_{lock}^*$  is the desired locking position for the angle that is kept locked. This additional constraint is different from the others already defined for the 3-panel system because it can only constrain one of the two shape angles at a time, thus acting as a sort of double constraint. From a mathematical point of view this requires that two analogous constraint Jacobian matrices are generated. During the simulation then it is sufficient to use a flag to select one of the two Jacobian matrices, that means specifying which of the shape angles  $\alpha_{ba}$  and  $\alpha_{cb}$  is either the locked or free angle at that specific instant in time. Adding this new constraints means that now the L-shape 3 panel array, already shown in Fig. 2.4, has only 4 DOF because either one of the hinges remains locked. In other words, when one of the angles is locked the system becomes a 2-body system with only one shape angle rotational DOF. This approach is much more computationally efficient than using the rotational spring solution but is less scalable to cases when the shape angles are more than two because it requires the generation of multiple Jacobian matrices.

A second numerical aspect that has to be taken into account when dealing with the modelling of 3D-multipanel arrays constrained with revolute joints is that for getting the shape angles

$\alpha_{ba}$  and  $\alpha_{cb}$  it is not sufficient to determine their sine using the cross products of Eq. (2.36) and (2.37) because this could indicate either an angle in the range  $[-90\ 90]$  [deg] or in the range  $[90\ 270]$  [deg]. This ambiguity leads to numerical discontinuities and non-physical behaviour of the model. For solving this issue it is necessary to also determine the sign of the cosine of the desired shape angle. This can be done by calculating the dot product of the two panel-fixed axes that are parallel to the revolute joint axis that the panels have in common. If these are oriented in the same direction that the cosine is positive and the desired shape angle is in the right quadrants, otherwise it is in the left quadrants.

By using the cosine of the shape angle as described we are basically adding a variable and the corresponding constraints that relates it to the other generalised coordinates. This is an example of an auxiliary variable. These variables can also be used for defining intermediate generalised coordinates, such as the elements of cross products, so that they appear in the constraints Jacobian matrix instead of the corresponding formulas that define them. The latter in fact, when derived, yields extremely long formulas that are not only hard to handle for symbolic calculus software but are also computationally inefficient.

### 3.3 Other Tools

In this Section some additional mathematical tools that have been exploited for the development of the multibody simulation environment and their specific use is discussed.

#### 3.3.1 Closed-Loop Feedback Control

In this thesis the system is controlled through an open-loop strategy. A reference shape angle sequence which is parametrized with respect to time is fed to the controller which, by interpolating it with current simulation time, retrieves a commanded shape angle. The hinge torques are then defined using a Proportional-Derivative control logic that drives to zero the error between the current value of the shape angle and the reference signal to be achieved:

$$\mathbf{u}(t) = \begin{bmatrix} -k_p (\alpha_{ba}(t) - \alpha_{ba}^*(t)) - k_d \dot{\alpha}_{ba}(t) \\ -k_p (\alpha_{cb}(t) - \alpha_{cb}^*(t)) - k_d \dot{\alpha}_{cb}(t) \end{bmatrix} \quad (3.5)$$

in which  $k_p$  and  $k_d$  have been manually tuned for minimum overshoot, settling error and settling time. For our specific configuration, by setting  $k_p$  and  $k_d$  both equal to 5 we obtain a settling time of 5.9 [s] for a settling error  $10^{-5}$  [rad]. More details about PD controllers can be found in [22].

### 3.3.2 Pseudospectral Local Optimization

Some of the results obtained in Section 4.1.1 are obtained by solving an optimal control problem. The objective in this case is to obtain preliminary internal torques reorientation trajectories for the multibody systems defined, eventually in case of path constraints. Among the many existing possibilities for achieving this it was chosen to exploit GPOPS-II [23].

GPOPS-II tool is based on local pseudospectral methods which belong to the class of direct methods. These are a family of algorithms whose aim is a clear and efficient discretization of the original optimal-control problem. The basic idea of these methods is to use of a particular set of nodes in which the states and the control are discretized. The optimal control problem transcription in this case defines an equivalent problem featuring a finite number of variables and constraints. The solution of this Nonlinear Programming Problem (NLP) approximates the continuous one. Pseudospectral methods are becoming more popular recently and are being applied in fields such as satellite attitude manoeuvring [24] and entry guidance [25].

In particular, GPOPS-II implements the Legendre-Gauss-Radau quadrature orthogonal collocation method where the continuous-time optimal control problem is transcribed to a large sparse NLP problem. The number of mesh intervals and the degree of the approximating polynomial within each mesh interval to achieve a specified accuracy is determined by means of an adaptive mesh refinement method. GPOPS-II can interface with both quasi-Newton (first derivative) and Newton (second derivative) nonlinear programming solvers. Also, it approximates all derivatives required by the nonlinear programming solver using sparse finite-differencing of the optimal control problem functions.

### 3.3.3 Newton-Raphson Root Estimation Method

For the purpose of simulating a mechanical system it is necessary to define initial values for its state variables. In principle one can specify the independent coordinates and determine the remaining dependent ones by means of the available constraints. It is possible however that the constraint equations are nonlinear or that solving the system of these many equations analytically is a process too lengthy. This is the case when simulating the 3D multipanel model for which it is desirable to define the initial state of the system by specifying the attitude quaternion of one of the panels and the two shape angles between them.

A time-efficient and accurate solution is to determine the remaining dependent coordinates, that are a function of the independent ones, using the Newton-Raphson method. This is a well-known numerical method that allows one find the unique solution of a system of equations within a specific interval. The iterative process starts with the determination of an initial guess  $\mathbf{x}_1$  for the solution to be found and then the updated solution  $\mathbf{x}_i$ , where  $i$  is the iteration index,

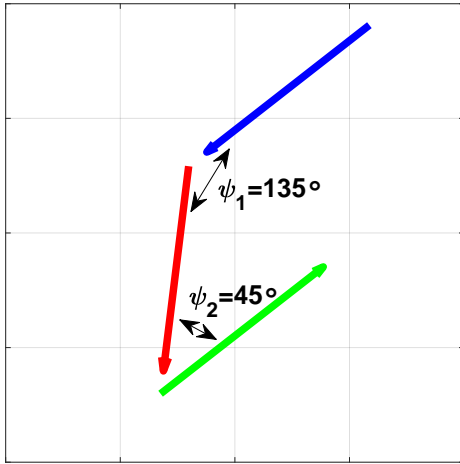


Figure 3.10: Situation of no-collision for an array of 3 rods of equal length.

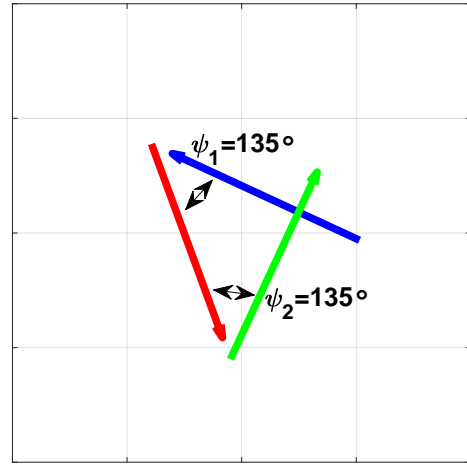


Figure 3.11: Situation of collision for an array of 3 rods of equal length.

is obtained as:

$$\mathbf{x}_{i+1} = \mathbf{x}_i - \mathbf{J}^{-1}\mathbf{F} \quad (3.6)$$

in which  $\mathbf{F}$  is the vector containing the equations of the system to be solved, that in this case are the constraints of the mechanical array, and  $\mathbf{J}$  the corresponding Jacobian matrix with respect to the variables to be approximated. The iterative process stops when the difference between two successive solutions is below a chosen accuracy threshold.

### 3.3.4 Collision Maps

A relevant problem for multibody arrays is impingement. The collision of two adjacent rods of the three rod chain can be avoided by constraining the range of the shape angles  $\psi_1$  and  $\psi_2$  to  $[-180^\circ, 180^\circ]$ . When the two external rods  $a$  and  $c$  (see Figure 2.3 for reference) are concerned, however, the collision area in the shape-plane depends on the relative lengths of all rods. Figure 3.10 and 3.11 show respectively the situations of no-impingement and impingement for the reference planar array of 3 equally long rods. In particular, collision domains in 2D can be obtained with an algorithm that establishes whether two segments intersect using the concept of orientation (clockwise, counter-clockwise or collinear) of triplets of extreme points [26]. Figure 3.12 shows half of the whole collision domain (the other half is clearly symmetric with respect to the origin) for different geometric configurations of the array. The domain disappears when  $l_b > l_a + l_c$ . For the 3D case the definition of the collision domain is a more complex and lengthy process and is not treated in this work. The main objective of this work is infact to characterize the basic behaviour of the class of underactuated systems defined above and the preliminary analysis of the 2D system in presence of collision constraints was considered to be sufficient for the purpose.

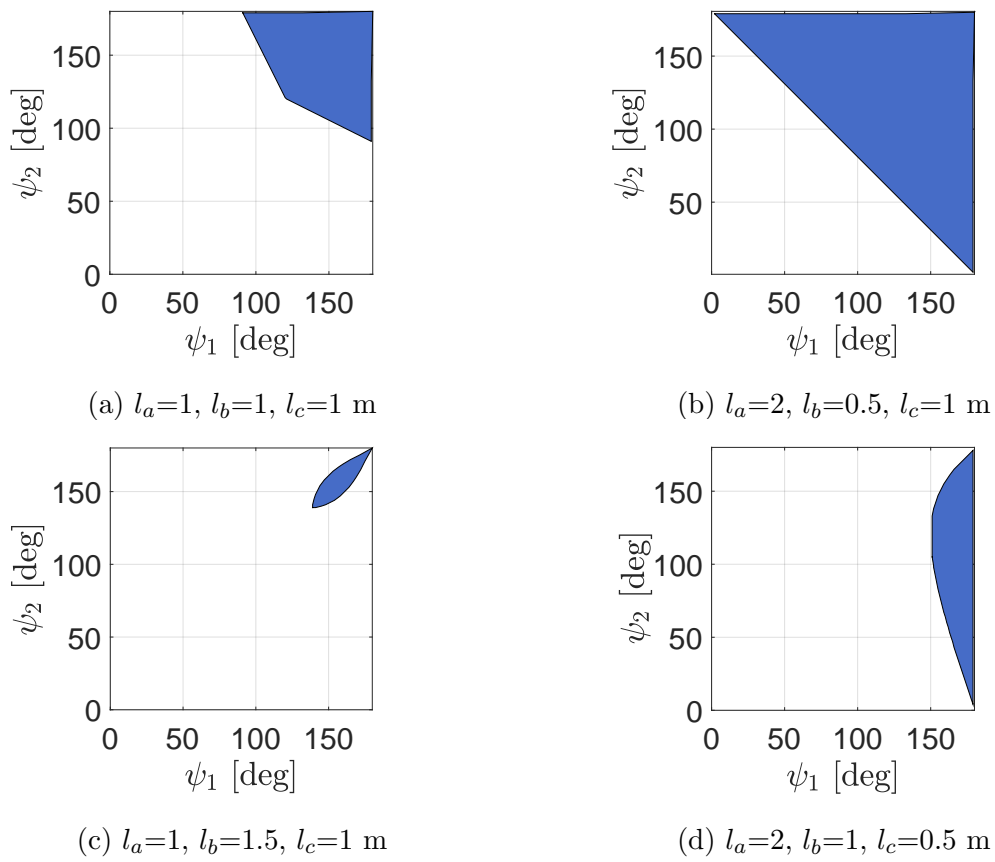


Figure 3.12: Collision domains (in blue) for different geometric configurations of the three rods array.

# 4 Results

This Chapter is dedicated to presenting the results obtained by simulating the motion of the multibody systems developed in Chapter 3. The focus, as already mentioned, is on understanding how it is possible to reorient an array in space by only exploiting internal torques that cause it to change its shape as part of the manoeuvre.

The approach consists in producing results that can be discussed in detail with the purpose of extracting interesting features of this class of underactuated control problem, whose dynamics are counter-intuitive because of the relevant role played by nonlinearities. In particular, the mechanics of the 3D system is much more complex because of the cross-couplings between rotational rates. However, the planar system already features the majority of the typical properties of this type of systems and is thus analysed first. The analysis of the 3D configuration extends these concepts to a configuration that has more complex behaviour and is closer to what could be applied for an operational system.

## 4.1 Planar Reorientation Trajectories

In this Section the three rod multibody model presented earlier is used to generate attitude reorientation trajectories that are significant for the research objectives discussed in Chapter 1. The manoeuvres taken into account are not only *rest-to-rest* but also *flat-to-flat*, which means that both at the beginning and at the end of the trajectory the COM of the rods are aligned and the chain is flat. The initial (dashed) and final (solid) states of the 3-rod planar array for a sample of such a trajectory is shown in Fig. 4.1. The assumptions *rest-to-rest* and *flat-to-flat* manoeuvre allow for easier comparison of while not affecting the physical meaning of the results. In fact, what is relevant is the overall angular variation  $\Delta\theta = \theta_{a,end} - \theta_{a,start}$  obtained, and the fact that the system has the same shape and total angular momentum at the beginning and at the end of the manoeuvre. The initial orientation can be chosen arbitrarily because there is no external dynamic contribution that depends on the state of the system. Section 4.1.1 will discuss optimal control trajectories and then in Sec. 4.1.2 the focus will be moved to the so-called rectangular reorientation manoeuvres which are named after their shape in the shape-angles domain and are particularly useful to understand the dynamical behaviour of the system.

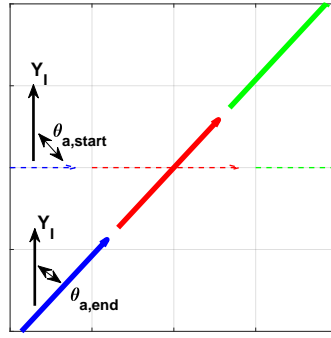
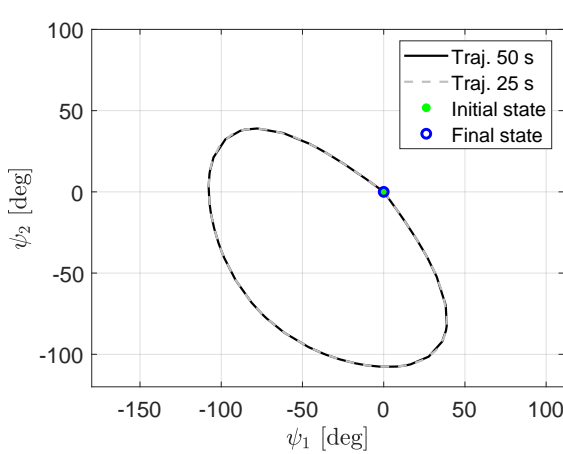
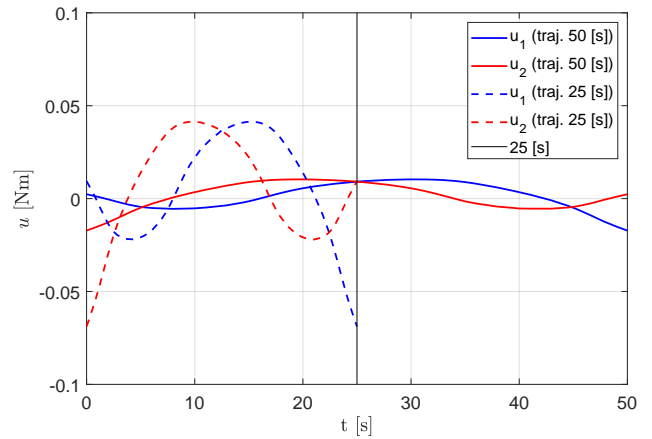


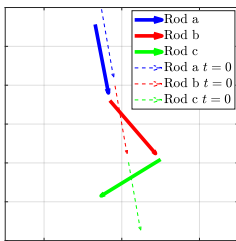
Figure 4.1: Initial (dashed) and final (solid) states of the 3-rod planar array for a sample *rest-to-rest* and *flat-to-flat* reorientation manoeuvre.



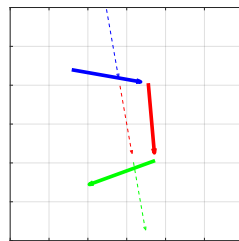
(a) Configuration paths in the shape-plane.



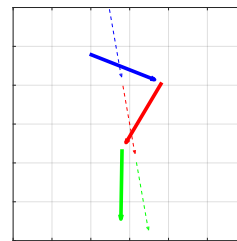
(b) Optimal control input sequences.



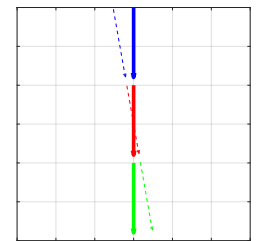
(c)  $t = 0.25t_M$ .



(d)  $t = 0.5t_M$ .



(e)  $t = 0.75t_M$ .



(f)  $t = t_M$ .

Figure 4.2: Comparison of optimal control effort trajectories correcting  $\Delta\theta=10^\circ$  in  $t_M=25$  s (dashed in Sub-figures (a,b)) and  $t_M=50$  s (solid in Sub-figures (a,b)). Dashed in Sub-figures (c,d,e,f) indicates the initial configuration of the rods which follow the same reorientation path in both cases.

### 4.1.1 Optimal Control Trajectories

The first exploratory results needed for understanding how to exploit internal joint torques for spacecraft attitude control have been gathered exploiting a numerical optimization approach. The objective of the manoeuvres here is to achieve a net desired reorientation  $\Delta\theta$  starting from an arbitrary initial attitude. Two types of reorientation trajectories for obtaining  $\Delta\theta$  in the range  $[-180^\circ, 180^\circ]$  have been tested, optimising either manoeuvre time or control effort using

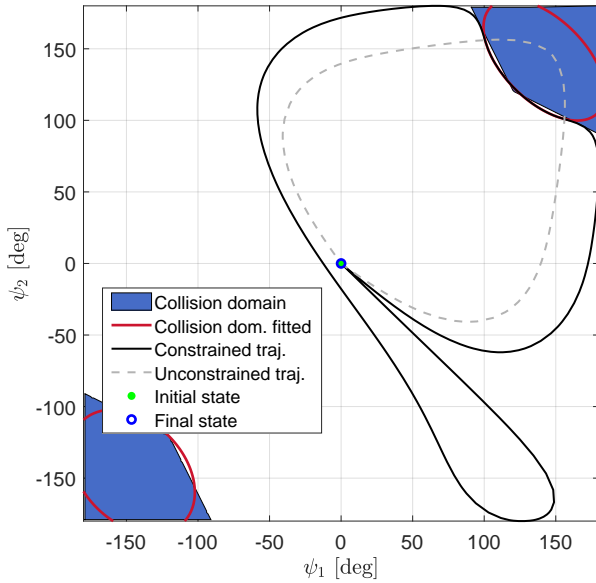
cost functions, respectively:

$$J = \int_{t_0}^{t_f} 1 dt; \quad J = \int_{t_0}^{t_f} \mathbf{u}^T \mathbf{I} \mathbf{u} dt; \quad (4.1)$$

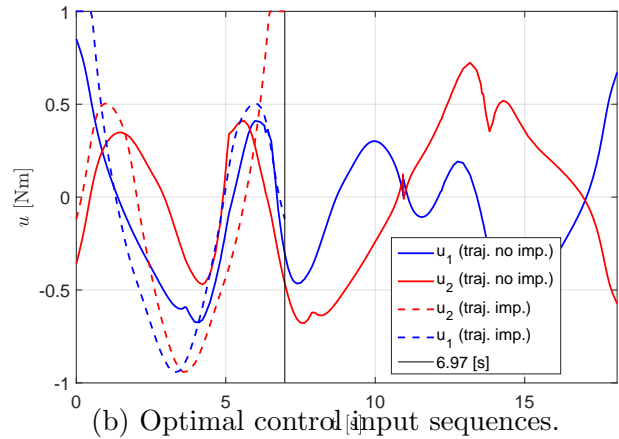
The control input sequences generated for minimum time manoeuvres, not unexpectedly, are *bang-bang* sequences. However, this is the case only when the control input range is small in relation to the inertia of the rods. The projection of *flat-to-flat* manoeuvres in the  $\psi_1\psi_2$ -plane, that will be defined as shape-plane or configuration space, are closed curves. Figure 4.2 shows that two minimum control effort manoeuvres with different durations and control input sequences that achieve the same net orientation change  $\Delta\theta=10^\circ$  follow the same path in the configuration space. This demonstrates that net orientation variation depends on the trajectory travelled in the shape angles-plane and not directly on the magnitude of the internal joint torques  $\mathbf{u}$ , which instead influences the control effort and duration of the manoeuvre. Analogous results in [16] were obtained using an analytical approach that finds a procedure to obtain a desired  $\Delta\theta$  as a function of the area enclosed by circular paths or other simple curves in the  $\psi_1\psi_2$ -plane, without considering path constraints. The problem of controlling the attitude of the three rod array can then eventually be separated in two parts. One consists of defining the path in the shape-angles configuration plane that generates the desired net change in orientation and the other part is to determine the control inputs that allow to get that path for a desired control effort and manoeuvre time.

Local pseudospectral optimization algorithms can only handle properly path constraints expressed by continuous functions so that the collision domains have to be defined accordingly if an optimal trajectory enforcing impingement avoidance has to be generated. A straightforward solution to this problem, that works satisfactorily only for some convex collision domains such as the one for the standard case in Figure 3.12a, is to approximate the forbidden area with an ellipse. Figure 4.3 shows the same minimum time manoeuvre reorientation trajectory with and without the collision avoidance constraint. The results demonstrate that the system is able to circumnavigate the obstacle but the path can become significantly more complex given the non-linear highly nature of the problem. A more in depth analysis of the performance of the system in case of external effects and path constraints, e.g., in terms of control effort and manoeuvre time variations, is recommended but is out of the scope of this thesis.

The optimal reorientation trajectories introduced show the peculiar dynamics of the array but obtaining such trajectories is an intensive task from the computational point of view. Using a standard Intel Core i7-7700 CPU @ 3.60 GHz Windows machine the optimization time for a *flat-to-flat* manoeuvre is in the order of minutes, and increases to tens of minutes when the collision avoidance path constraint is enforced.



(a) Configuration paths in the shape-plane.



(b) Optimal control input sequences.

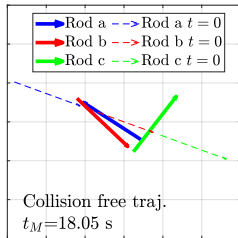
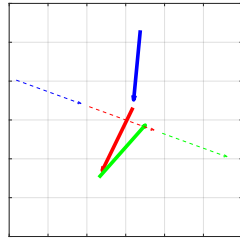
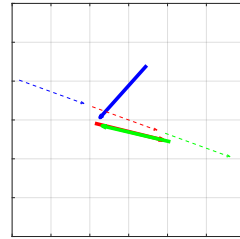
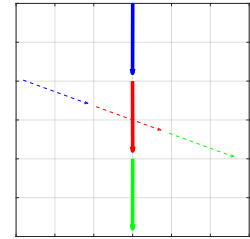
(c)  $t = 0.25t_M$ .(d)  $t = 0.5t_M$ .(e)  $t = 0.75t_M$ .(f)  $t = t_M$ .

Figure 4.3: Comparison of minimum time trajectories correcting  $\Delta\theta=70^\circ$  with (solid in Sub-figures (a,b)) and without (dashed in Sub-figures (a,b)) impingement avoidance constraint. Dashed in Sub-figures (c,d,e,f) indicates the initial configuration of the rods which follow the same reorientation path for both cases.

### 4.1.2 Rectangular Trajectories

Rectangular trajectories are named after their shape in the shape angles-domain. They consist of one of the shape angles varying while the other remains locked. These trajectories are very useful to gain a better understanding of the counter-intuitive dynamic behaviour of the system under analysis. Also, they allow to easily parametrize and map the reorientation achieved as a function of the shape angle variation.

Assume that the two internal shape angles are labelled  $\psi_v$  and  $\psi_w$ , where either  $[v, w] = [1, 2]$  or  $[v, w] = [2, 1]$ . Also assume that only one shape angle  $\psi_v$  at a time varies due to the application of the corresponding internal joint torque while the other angle  $\psi_w$  is locked in position  $\psi_{w,0}$ , where the second index, 0 in this case, indicates the locking position. In the configuration space, i.e. the  $\psi_1\psi_2$ -plane, the trajectory going from  $\psi_{v,0}$  to  $\psi_{v,1}$ , is a segment parallel to the horizontal axis if  $v = 1$  or to the vertical axis if  $v = 2$ . This motion, in agreement with the law of conservation of angular momentum, results in a variation of the orientation angle  $\Delta\theta_{a,1}$ .

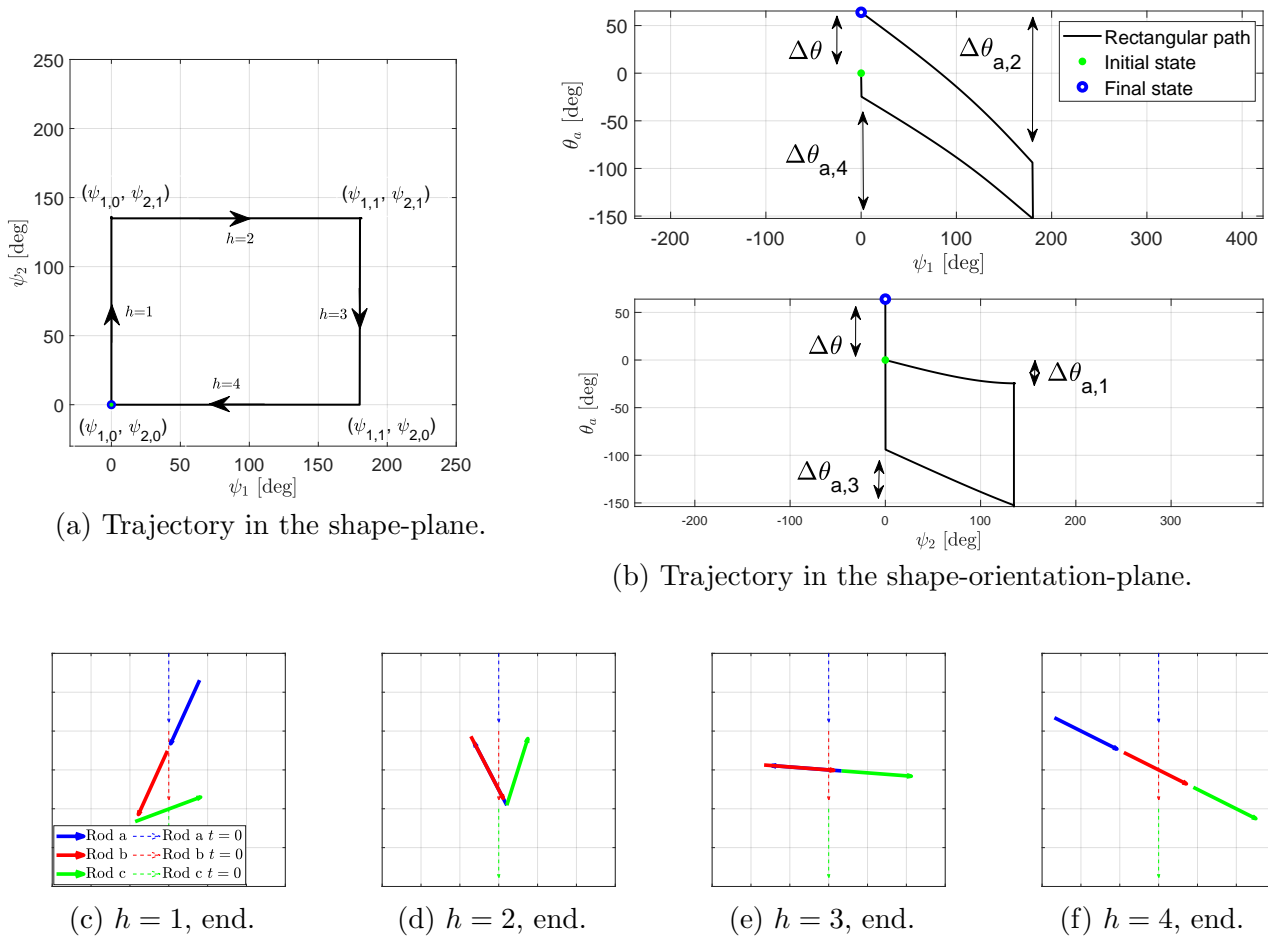


Figure 4.4: Clockwise rectangular *flat-to-flat* reorientation manoeuvre.

At the end of this first segment  $\psi_v$  gets locked in position  $\psi_{v,1}$  and  $\psi_w$  is unlocked and brought from  $\psi_{w,0}$  to  $\psi_{w,1}$ , where again it gets locked. Then,  $\theta_a$  is subjected to a variation  $\Delta\theta_{a,2}$ . The third and fourth segments are respectively given by  $\psi_v$  going from  $\psi_{v,1}$  back to  $\psi_{v,0}$ , with  $\psi_w$  locked in position  $\psi_{w,1}$  and  $\psi_w$  going from  $\psi_{w,1}$  back to  $\psi_{w,0}$ , with  $\psi_v$  fixed to  $\psi_{v,0}$ . While the array configuration travels along these two segments the orientation angle of rod  $a$  changes by  $\Delta\theta_{a,3}$  and  $\Delta\theta_{a,4}$ . The net change in absolute orientation of the system at the end of the path is:

$$\Delta\theta = \Delta\theta_{a,1} + \Delta\theta_{a,2} + \Delta\theta_{a,3} + \Delta\theta_{a,4} \quad (4.2)$$

that, assuming *flat-to-flat* manoeuvres ( $\psi_{v,0} = \psi_{w,0} = 0$ ), exclusively depends on  $\psi_{v,1}$  and  $\psi_{w,1}$  and on the direction the path is travelled, clockwise ( $v = 1, w = 2$ ) or anticlockwise ( $v = 2, w = 1$ ). In particular, the same rectangular path travelled in opposite directions yields the opposite  $\Delta\theta$ . Figure 4.4 shows the rectangular reorientation trajectory described travelling clockwise.

The problem of determining the input joint torque that allows the chosen reorientation trajectory to be followed, that as noted earlier can be treated separately, can be solved easily for the case of rectangular manoeuvres. A proportional-derivative control law drives the array along each segment:

$$u_j = -k_p(\psi_j - \psi_j^*) - k_d\dot{\psi}_j \quad (4.3)$$

where  $\psi_j^*$  is the shape angle to reach at the end of the segment. The gains  $k_p$  and  $k_d$  have been optimised by means of a step response analysis for the default system mass and geometry to achieve minimum settling time with no overshoot. Each side of the rectangle takes the same time to be travelled.

To obtain a better understanding of the dynamics of the array consider that an arbitrary segment  $h$  between  $\psi_{v,start}$  and  $\psi_{v,end}$ , with  $\psi_w$  locked in position  $\psi_{w,lock}$  describes the motion of a  $N = 2$  multibody array. One of the two rigid-bodies is the two rods interconnected by joint  $w$  while the other is the remaining rod. The two rods rigidly linked have a specific moment of inertia that depends on the lock angle position  $\psi_{w,lock}$  and determines how the orientation angle  $\theta_a$  varies as a function of  $\psi_v$ . The following relationship, determined by fitting the trajectory data with a polynomial, holds true:

$$\Delta\theta_h = f_h(\psi_{v,end}) - f_h(\psi_{v,start}), \quad f_h(\psi_v) = b_1\psi_v + b_2\sin(b_3\psi_v + b_4) + b_5 \quad (4.4)$$

in which the average slope  $b_1$  and the other parameters  $b_{2-4}$  depend on the mass and geometric properties of the array and on  $\psi_{w,lock}$  while  $b_5$  is determined by the initial conditions of the segment. The function  $f_h$  has been estimated numerically for different shape angle lock positions of the default array configuration and is given in Figure 4.5 for  $v = 1, w = 2$ . In agreement with the law of conservation of angular momentum, when the two rods linked rigidly are folded in on themselves ( $\psi_{w,lock} = 180^\circ$ ) the moment of inertia of the rigid element they make is lower and the same  $\Delta\psi_v = \psi_{v,end} - \psi_{v,start}$  yields a larger  $\Delta\theta_{a,h}$ .

From what has been observed until now, it can be stated that the direction of the overall

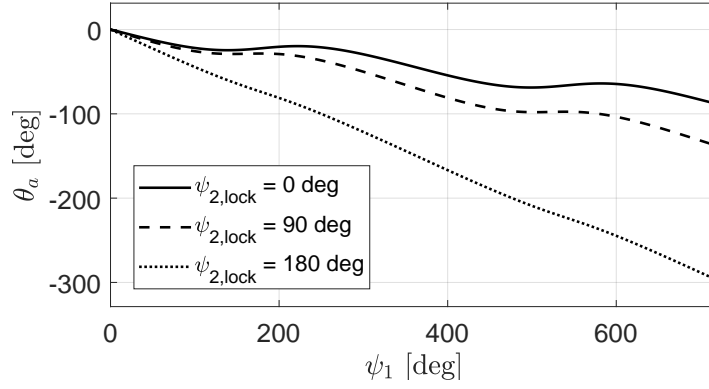


Figure 4.5: Variation of  $\theta_a$  as a function of  $\psi_1$  for different lock angle positions  $\psi_{2,lock}$  and  $b_5 = 0$ .

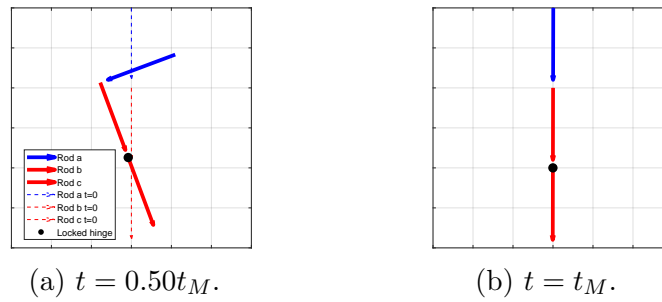


Figure 4.6: Shape angle *flat-to-flat* manoeuvre for  $N < 3$  array achieving no reorientation.

orientation variation for a rectangular path depends on the direction the path is travelled and the magnitude of this variation is a function of the area that is enclosed in the rectangle<sup>1</sup>. If this area is null then at the end of the manoeuvre the array goes back to its initial conditions. This happens for example if, just after reaching  $\psi_{v,1}$ , the angle  $\psi_v$  is brought back to initial position  $\psi_{v,0}$ , while always keeping  $\psi_{w,0}$  locked so that the full manoeuvre path in the  $\psi_1\psi_2$ -plane encloses no area and the net change in  $\theta_a$  is null. If one hinge is locked then the number of modules is  $N = 2$ , and the system is equivalent to a 2-rods array. In such case the specific moments of inertia of the 2 linked elements is the same for both segments so that they have the same  $f_h$  and achieve exactly the opposite  $\Delta\theta_{a,h}$  going back and forth between the extremes. This is the reason why there is no *rest-to-rest* manoeuvre that achieves absolute reorientation for a planar multibody system with  $N = 2$ . The situation described is shown in Figure 4.6.

The situation is different when we have  $N = 3$  modules. In fact, before  $\psi_v$  is brought back to its initial condition  $\psi_{v,0}$  as a result of the third segment of the rectangular trajectory, the angle  $\psi_w$  has gone from  $\psi_{w,0}$  to  $\psi_{w,1}$  with the result that the moment of inertia of the block of two rods interconnected by hinge  $w$  has changed. The parameters of  $f_h$ ,  $b_1$  in particular, are not the same for the two parallel segments travelling in opposite directions. In summary, the net change in absolute orientation obtained at the end of the manoeuvre described is due to a

<sup>1</sup>This holds assuming rectangular trajectories. For trajectories of different shape the net reorientation would depend on other parameters that relate to that specific shape. For a rectangular trajectory the area enclosed is a parameter easy to evaluate but for other shapes this could not be the case.

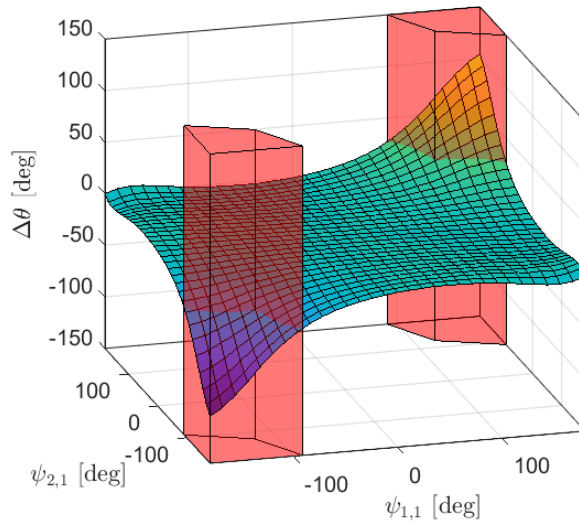


Figure 4.7: Net reorientation for different *flat-to-flat* clockwise rectangular manoeuvres. The red prisms contain those shape-angles configurations of the reference system that are not feasible due to rods impingement.

nonlinear dynamic effect caused by the variable inertia of the array. This effect is particularly evident for the rectangular path analysed, but the same physical concept applies in general to all *rest-to-rest* manoeuvres such as those in Figure 4.2 and 4.3.

Finally, Figure 4.7 shows how  $\Delta\theta$  for a clockwise rectangular *flat-to-flat* manoeuvre varies as a function of the two shape angles positions characterising it,  $\psi_{1,1}$  and  $\psi_{2,1}$ . The red prisms contain those shape angle configurations that are not feasible due to rod collision. As expected, the larger the difference in the moment of inertia of the array when parallel opposite segments are travelled, the larger the  $\Delta\theta$  that can be obtained. Also, given a desired  $\Delta\theta$ , the function in Figure 4.7 can be interpolated to obtain the corresponding set of  $\psi_{1,1}$  and  $\psi_{2,1}$  that allow us to achieve this change in orientation. The same function can additionally be used for building trajectories that patch together multiple rectangular paths for reaching any planar attitude condition.

## 4.2 3D Reorientation Trajectories

As already discussed, 3D reorientation manoeuvres are much more complex than planar ones because of the rotational rate cross-couplings that the system experiences. This makes its kinematic behaviour less intuitive than for the 2D case. Nevertheless, the same reorientation concepts based on the exploitation of momentum-preserving internal torques can be applied and analogous results can be obtained. Figure 4.8 shows the sequence of sequential shapes for a sample 3D rectangular reorientation trajectory of 40 [s] divided in sections of 10 [s] each during which one of the shape angles has a variation of  $90^\circ$ .

Also for the 3D L-shape system a sample database of rectangular trajectories, i.e., parametrized with respect to 2 shape angles, was built. This array, however, does not only rotate in the plane

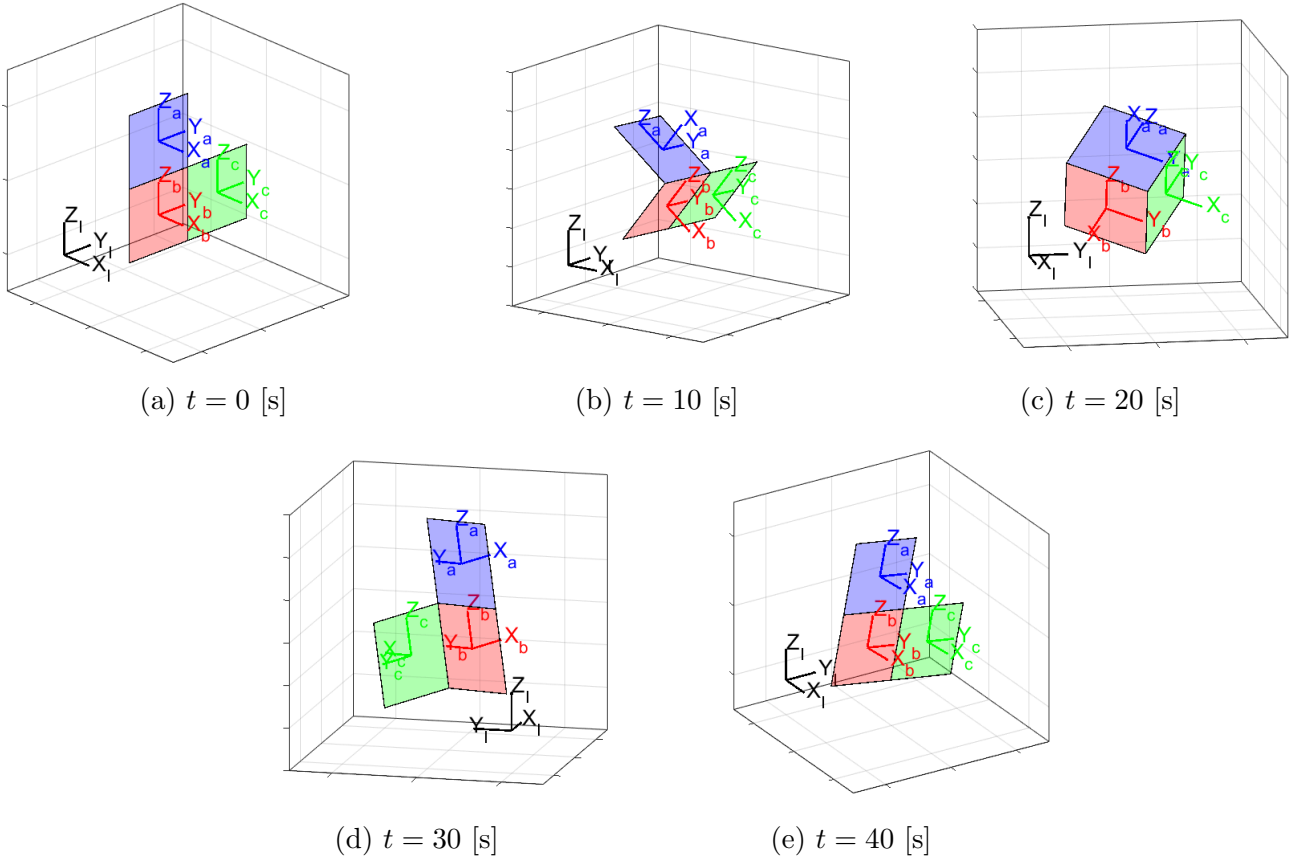


Figure 4.8: L-shape array performing a 3D *flat-to-flat* rectangular reorientation manoeuvre.

but in 3 dimensions, meaning that at least 3 independent quantities are needed for parametrizing a non-holonomic turn. These can be Euler angles but a more appropriate representation, already exploited in [13], is the axis-angle formalism introduced in Chapter 2. Using this approach each flat-to-flat non-holonomic turn, generated by the system following a commanded rectangular path in the shape-angle plane, results in a precise rotational direction and a rotation angle around it.

The attitude of the system is propagated in quaternions for numerical efficiency reasons. The non-holomic turn in terms of this attitude representation is found by multiplying the attitude quaternion at the beginning of the manoeuvre by the conjugate of the quaternion at the end of the manoeuvre:

$$d\mathbf{q}_{\text{NHT}} = \text{quatmultiply}(\mathbf{q}_{\text{NHT, end}}, \mathbf{q}'_{\text{NHT, start}}) \quad (4.5)$$

The change in attitude in terms of rotation axis and angle around it is given by simply transforming  $d\mathbf{q}_{\text{NHT}}$  from a quaternion to an axis-angle representation. For comparing the 3D non-holonomic turns a spherical plot was chosen. In this plot the position of the points on the sphere gives the direction of the rotation axis. Their colour indicates the efficiency of the turn that is defined as the product between the angular distance  $\theta_{\text{NHT}}$  around the non-holonomic turn rotation axis and the inverse of the angular shape distance covered:

$$\text{eff}_{\text{NHT}} = \frac{\theta_{\text{NHT}}}{2(\Delta\psi_1 + \Delta\psi_2)} \quad (4.6)$$

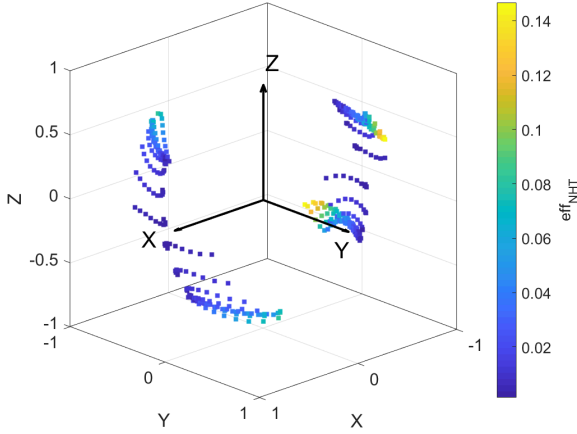


Figure 4.9: L-shape multipanel system non-holonomic turn direction and efficiency.

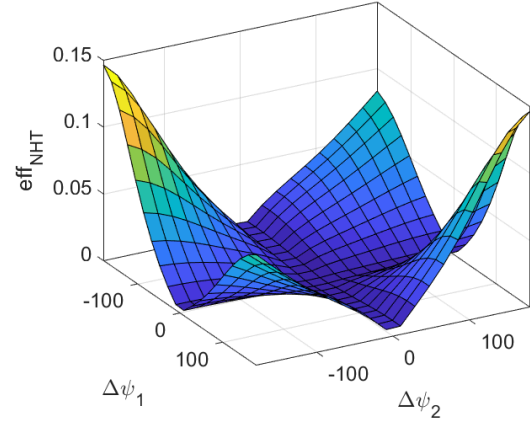


Figure 4.10: L-shape multipanel system non-holonomic turn efficiency as a function of shape angle variation.

Figure 4.9 gives the reorientation directions for a set of 400 sample rectangular non-holonomic turn rectangular trajectories followed clockwise (first  $\psi_1$  varies) obtained by sampling both  $\Delta\psi_1$  and  $\Delta\psi_2$  in the interval  $[-180^\circ 180^\circ]$ . All the reorientation manoeuvres start from the condition of Figure 4.8 (a). Figure 4.9 shows clearly that the array cannot reorient, with a single rectangular manoeuvre, in any direction. Also, it is clear that the most efficient reorientation trajectories only cover specific directions.

The same set of 400 samples is depicted in Figure 4.10 which shows the non-holonomic reorientation efficiency as a function of  $\Delta\psi_1$  and  $\Delta\psi_2$  total variations. It is clear that, analogously to the planar case, also in the 3D case the better efficiency, the largest reorientation angular distance is obtained for the cases in which the difference in terms of moment of inertia of the array between two parallel segments is larger, as explained in the previous Sections. This happens, as expected, for shape angle variations close to  $180^\circ$  corresponding to the case in which two panels of the array fold together starting from the flat unfolded condition. A third relevant plot that was obtained with the same set of 400 sample trajectories is shown in Figure 4.11. This plot shows how the direction of the body axes of one of the panels, which is equivalent to that of the others when the array is in a flat configuration, varies after the non-holonomic turn manoeuvre. This plot confirms that there exist some preferential rotation directions that can be achieved by the array using this reorientation mechanism. These preferential directions depend on the characteristics of the array.

A relevant remark has to be made concerning the fact that the rectangular trajectories followed in the opposite direction to those shown, i.e., counter-clockwise, generate plots that are mirrored with respect to those shown above. This behaviour is analogous to that already observed for the planar case. Finally, it has to be noted that with a proper selection of sequential non-holonomic turns, in principle it could be possible to achieve a larger range of array orientations. In fact, after one turn has been realised the set of axes rotates accordingly on the surface of the orientation sphere. In other words, the  $\chi$ -like point clouds that we see in Figure 4.11 shift and

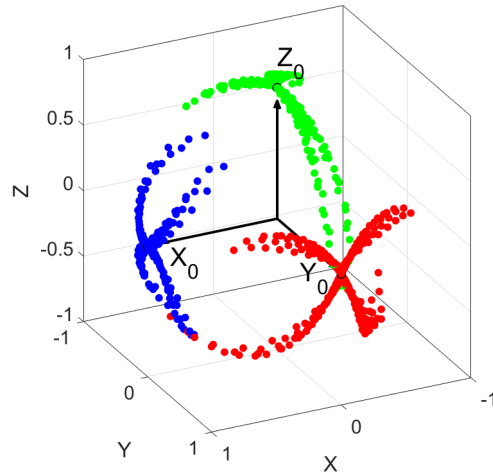


Figure 4.11: Multipanel system body axes directions after non-holonomic turns (X-axis is blue, Y-axis is red, Z-axis is green).

are now centred on the new directions of the  $XYZ$ -axes of the array. This suggests that it is possible to find a sequence of *flat-to-flat* reorientation manoeuvres that can rotate the axes of the array from the initial attitude  $X_0Y_0Z_0$  to arbitrary attitude conditions within a particular range. Similarly, it was also possible for the previously discussed planar 3-rods array to achieve any reorientation angle in the range  $[0\ 360^\circ]$  by performing a planned sequence of rectangular manoeuvres, or a sequence of any other type of closed-path manoeuvres in the shape-angles domain. The range of achievable orientations that can be achieved by the 3D array, however, depends on the properties of the array, including the number of modules, their inertia and geometric properties, the hinges it has and how these modules can move with respect to each other.

# 5 Conclusions & Recommendations

The present Chapter summarises the information and results presented up to this point and suggests possible research directions to undertake on the base of these findings.

## 5.1 Conclusions

The present study has presented multiple phases. First of all, it gathered together the available information and literature regarding the exploitation of internal torques for control purposes. From the literature study summarized in Chapter 1 it is clear that the topic is of great interest for space applications. In fact, the high costs characterising any space mission are pushing for the development of technological solutions that increase the efficiency and versatility of systems. A possible solution is an array that requires a low amount of energy for controlling its own state, thanks to the use of internal torques. The envisioned system would be able to reconfigure its shape for complying with the requirements of a larger number of orbital functions with respect to existing systems. It could revolutionise classes of small satellite missions and ensure a cheaper access to space for instrumentation testing or scientific data harvesting.

Reconfigurable systems represent the state of the art of robotics. At the moment many concepts are being investigated and tested even if an application that would justify the increased development cost, with respect to fixed configuration systems, that perform optimally for a specific task, has not been identified yet. This application, for the reasons introduced above, could be the used in space. Nevertheless, space systems are required to ensure high robustness. State of the art reconfigurable systems are still limited and the advantages of this technology, as well as its flaws, are still unknown. This is especially because of the non-linearities that dominate their behaviour which prevent the use of classical control approaches which dominate space technology which remains resilient to tried-and-tested solutions. From this it follows that a better understanding of the peculiar behaviour and dynamics of reconfigurable system, with a particular focus on what a space system of this type could look like, represents a necessary step for the future operational space scenarios.

The second step consisted in the development of a validated simulation tool and a framework that allows the extraction of information about the most peculiar traits of internal torques whose behaviour, as already mentioned, is highly non-linear and thus unintuitive. This development

required high-level multibody mechanics and the solution of some issues related to the numerical stability and computational efficiency of the simulation for both the planar and, then, the 3D case which is significantly more critical in terms of complexity. The resulting tools simulate respectively the motion of a sequence of rods in 2D and that of an L-shape multipanel array in 3D. The dynamics of both these configurations are relevant for a multipanel cube which is assumed to be the reference case for a reconfigurable system for space applications. The simulation tool does not only allow the investigation of how the system responds to internal control torques but can easily be adapted to different configurations from those studied here and can be extended with more modules eventually featuring different mass/inertia properties or producing/responding to forces.

The third and final step of the thesis, starting from the information gathered during the literature review, exploited the potentialities of the multibody simulation tools for determining the characteristic behaviour of the reference array in both 2D and 3D domains. This study proved the feasibility of the concept and documented some valid reorientation strategies that represent a baseline to be expanded and modified depending on the specific characteristics and needs of the reconfigurable system that has to be developed.

## 5.2 Recommendations

One of the major achievements of this work consisted in identifying some critical points and research directions to follow for generating the results that could be most relevant for a future implementation of internal torques attitude control and shape reconfiguration technology for space applications:

1. Even if the results gathered here are valid in general for any reconfigurable systems exploiting internal torques for reorientation purposes, arrays that do not comply with the assumptions made for the reference system could reveal different behaviours. For example if the centres of gravity of the panel modules are not aligned then also the motion of three panels in the chain configuration would generate an off-plane rotation of the system. Different rotational behaviours would also be experienced if the panels are constrained along their sides, but can rotate about the axes perpendicular to it or if these can translate relative to each other.
2. The reorientation maps that have been produced are valid for a specific array configuration. Each base configuration of the panels/rods will result in a different map. If an array is composed of more than three elements an interesting solution for its attitude control is to define reorientation maps for different combinations of groups of panels moving relative to each other. This would add various options for the internal angles control trajectory that can be followed for reorientation between two fixed attitude conditions.
3. In Chapter 4 it was verified that a reorientation trajectory in the shape-angles plane is

- a closed path enclosing a non-null area. The focus was on rectangular reorientation trajectories because they represent the most appropriate option to understand the dynamic behaviour of this class of underactuated systems, which is the primary objective of this thesis. However, the solution of the optimal control problem has shown that the control input sequence in the shape-angle domain that minimizes control effort is not a rectangle but can have different shapes, still enclosing a non-null area, depending on the constraints and the properties of the system. This suggests that it could be possible to design reorientation trajectories in the shape-angle domain that can be still parametrized easily, such as ovals, circles or other more complicated closed shapes, but can be more efficient than rectangular ones with respect to some specific reorientation tasks.
4. It was verified that a planar array made of at least three rods can achieve any orientation in the range  $[0^\circ \ 360^\circ]$  by following a sequence of single reorientation trajectories that in the shape-angle domain are closed paths of arbitrary shape enclosing a non-null area. For the 3D case the determination of the range of possible orientation, that can be achieved by exploiting internal torques is more complicated due to the kinematic coupling that characterises 3D multibody systems. In any case, this range is limited by the properties of the array, including the number of modules, their inertia and geometric properties, the hinges it has and how the modules of the array can move with respect to each other.
  5. The interest in the field of underactuated control problems, of which internal torque reorientation in space is an example, has been growing sharply in the last few years in parallel with the developments in the field of Artificial Intelligence. In fact, despite the advantages internal torques can yield, their behaviour is highly nonlinear and unintuitive. Mathematical methods such as neural networks represent a promising option for the development of control algorithms for this type of system. Some tests of network training were conducted within this research work but the performance achieved by the algorithm was low and the increase in system complexity not needed, especially for the 2D case where the reorientation trajectory can be determined by simply interpolating the map. It is believed however that an increase in the number of modules and the need for 3D reorientation control could optimally exploit the advantages of neural networks that can be trained using previously built reorientation maps.
  6. The array mechanics simulations that have been run were aimed at isolating the effect of internal torques on the array attitude. Nevertheless, it is possible to extend the model to also include external dynamic contributions such as solar radiation pressure and drag or gravity gradient. These additions would significantly increase the complexity of the system and produce completely different reorientation maps. The same can be achieved by including the effect of thrusters or other actuators that can be used in synergy with internal torques.
  7. Impingement avoidance has been analysed for the 2D planar system. The definition of this problem increases in terms of complexity with the number of modules involved in the manoeuvre. This is especially true for 3D-reorientations. The solution of the reorientation

problem, apart from the case of simple trajectories in which efficiency is not a concern, can be found by exploiting a motion planning approach.

8. The active use of the shape of the array could allow the control of the orientation of each module singularly. This would be useful for example in the situation in which the system has to support multiple payloads pointing at different targets in 3D space.
9. The simulation environment developed using the multibody methodology presented can serve as a kernel for an extended tool that can simulate the motion of systems featuring a larger number of modules.

# Bibliography

- [1] J. Kawaguchi, K. Ohashi, and Y. Kubo. Keynote : On Non-Holonomic Attitude Control Scheme Applied to Transformable Spacecraft. *5th International Symposium on Solar Sailing*, 2019.
- [2] Qiao Qiao, Jianping Yuan, Mingming Wang, and Xin Ning. Attitude control of a picosatellite named NPU-PhoneSat based on shape actuation. *Aerospace Science and Technology*, 71:62–67, 2017.
- [3] Reyhanoglu M. and N. H. McClamroch. Controllability and Stabilizability of Planar Multi-body Systems with Angular Momentum Preserving Control Torques. In *Proceedings of 30th IEEE Conference on Decision and Control*, 1991.
- [4] J. Bouwmeester and J. Guo. Survey of worldwide pico- and nanosatellite missions, distributions and subsystem technology. *Acta Astronautica*, 67(7-8):854–862, 2010.
- [5] Mark Yim, Wei Min Shen, Benham Salemi, Daniela Rus, Mark Moll, Hod Lipson, Eric Klavins, and Gregory S. Chirikjian. Modular self-reconfigurable robot systems [Grand challenges of robotics]. *IEEE Robotics and Automation Magazine*, 14(1):43–52, 2007.
- [6] Joseph Shoer and Mason Peck. Reconfigurable Spacecraft as Kinematic Mechanisms Based on Flux-Pinning Interactions. *Journal of Spacecraft and Rockets*, 46(2):466–469, 2009.
- [7] Martin N Nisser, Dario Izzo, and Andreas B Orggraeffe. An Electromagnetically Actuated , Self-Reconfigurable Space Structure. *JSASS Aerospace Tech. Japan*, 14:1–9, 2017.
- [8] Ariel Ekblaw and Joseph Paradiso. Self-assembling Space Structures: Buckminsterfullerene Sensor Nodes. *2018 AIAA/AHS Adaptive Structures Conference*, (January), 2018.
- [9] Zhenishbek Zhakypov and Jamie Paik. Design Methodology for Constructing Multimaterial Origami Robots and Machines. *IEEE Transactions on Robotics*, 34(1):151–165, 2018.
- [10] Rainer Sandau. Status and trends of small satellite missions for Earth observation. *Acta Astronautica*, 66(1-2):1–12, 2010.
- [11] I. Nann and S. Abbondanza. Nanosatellites: What can they really do? In *Proceedings of the 4S Symposium - Small Satellites Systems and Services*, page 33, Rhodes, Greece, 2008.

- [12] T.R. Kane and M.P. Scher. A dynamical explanation of the falling cat phenomenon. *International Journal of Solids and Structures*, 5(7):663–670, 1969.
- [13] Kaoru Ohashi, Toshihiro Chujo, and Junichiro Kawaguchi. MOTION PLANNING IN ATTITUDE MANEUVER USING NON - HOLONOMIC TURNS FOR A TRANSFORMABLE SPACECRAFT. In *28th Workshop on JAXA Astrodynamics and Flight Mechanics*, 2018.
- [14] M Reyhanoglu and N McClamroch. Reorientation of space multibody systems maintaining zero angular momentum. *Proceedings of the AIAA Guidance, Navigation and Control Conference. Part 1 (of 3), Aug 12 - 14 1991*, 1:1330, 1991.
- [15] M. Reyhanoglu and N H. McClamroch. Planar reorientation maneuvers of space multibody systems using internal controls. *Journal of Guidance, Control, and Dynamics*, 15(6):1475–1480, 1992.
- [16] Gregory C Walsh and S Shankar Sastry. On Reorienting Linked Rigid Bodies Using Internal Motions. *IEEE TRANSACTIONS ON ROBOTICS AND AUTOMATION*, 11(1), 1995.
- [17] N. Sreenath. Nonlinear control of planar multibody systems in shape space. *Mathematics of Control, Signals, and Systems*, 5(4):343–363, 1992.
- [18] P S Krishnaprasad. Geometric Phases, and Optimal Reconfiguration for Multibody Systems. *American Control Conference, 1990*, pages 2440–2444, 1990.
- [19] E. Mooij. *Re-entry Systems: Lecture Notes Course AE4870B*. Delft University of Technology, 2015.
- [20] R.A. Wehage and E.J. Haug. Generalised Coordinate Partitioning In Dynamic Analysis of Mechanical Systems. Technical report, U.S. Army Tank-Automotive Command Research and Development Center, 1980.
- [21] Ahmed A. Shabana. *Dynamics of Multibody Systems*. Cambridge University Press, 2005.
- [22] K. Ogata. *Modern control engineering*. Prentice-Hall, 2010.
- [23] M. A. Patterson and A. V. Rao. GPOPSII: A MATLAB Software for Solving Multiple-Phase Optimal Control Problems Using hp-Adaptive Gaussian Quadrature Collocation Methods and Sparse Nonlinear Programming. *ACM Transactions on Mathematical Software*, 41(1), 2014.
- [24] Zhang Y. Li W. Zhang, W. and Y. Wang. Path Planning for Rapid Large-Angle Maneuver of Satellites Based on the Gauss Pseudospectral Method. *Hindawi Publishing Corporation*, 2016.
- [25] M. Sagliano and E. Mooij. Optimal Drag-Energy Entry Guidance via Pseudospectral Convex Optimization. *AIAA Scitech Forum, Guidance Navigation and Control Conference*, 2018.

- [26] Thomas H Cormen, Charles E Leiserson, Ronald L Rivest, and Clifford Stein. Determining whether any pair of segments intersects. In *Introduction to Algorithms*, chapter 33, pages 935–940. MIT Press and McGraw-Hill, second edition, 2001.